Matrix Isolation and *ab initio* studies of Propofol: Conformational Analysis and Hydrogen Bonding Interactions

Srijit Mukherjee

MS11006

A dissertation submitted for the partial fulfillment of BS-MS dual degree in Science

Indian Institute of Science Education and Research Mohali

April 2016

Certificate of Examination

This is to certify that the dissertation titled "Matrix Isolation and *ab initio* studies of Propofol: Conformational Analysis and Hydrogen Bonding Interactions" submitted by Mr. Srijit Mukherjee (Registration Number: MS11006) for the partial fulfillment of BS-MS dual degree program of IISER Mohali, has been examined by the thesis committee duly appointed by the Institute. The committee finds the work done by the candidate satisfactory and recommends that the report be accepted.

Dr. Sugumar Venkatramani Dr P. Balanarayan Dr. K. S. Viswanathan

Dated: April, 22, 2016

Declaration

The work presented in this dissertation has been carried out by me under the guidance of Prof. K. S. Viswanathan at the Indian Institute of Science Education and Research Mohali. This work has not been submitted in part or in full for a degree, a diploma, or a fellowship to any other university or institute. Whenever contributions of others are involved, every effort is made to indicate this clearly, with due acknowledgement of collaborative research and discussions. This thesis is a bonafide record of original work done by me and all sources listed within have been detailed in the bibliography.

Srijit Mukherjee
MS11006
(Candidate)
Dated: April 22, 2016

In my capacity as the supervisor of the candidate's project work, I certify the above statements by the candidate are true to the best of my knowledge.

Prof. K. S. Viswanathan
(Supervisor)

Acknowledgements

First and foremost, I draw a sense of profound gratitude, acknowledgement and admiration towards my thesis supervisor Prof. K. S Viswanathan. I am much obliged to thank him for being my mentor, teacher and for guiding me in and all. From discussions to valuable advice, Prof. Viswanathan, has truly been the pillar who has supported and encouraged me throughout the duration of this project. I also thank Dr. Sugumar Venkatramani and Dr. P. Balanarayan for being a part of my thesis committee and for always being available for invaluable discussions and suggestions. I also thank Dr. Arijit Kumar De and Prof. N. Sathyamurthy for discussions and valuable suggestions from time to time.

I express my sincerest gratitude and acknowledgement to all my lab members- Kanupriya Verma, Ginny Karir, Pankaj Dubey, Jyoti Saini and Dr. Anamika Mukhopadhyay. Their presence and help was critical in understanding the working of the MI-FTIR setup and developing an essence for the research problem that I was interested to pursue. I thank them to set up an environment of professionalism and positivity that has continually boosted my confidence in research.

I am grateful to my parents, Mrs. Rita Mukerji and Mr. Swapnajit Mukerji. Their role has been instrumental in the development and shaping of my academic career. Their support and encouragement has allowed me to pursue a career in basic sciences with confidence, zeal and enthusiasm.

Most importantly, I need to thank a long list of friends who have been the epicentre for my healthy performance and activity. From valuable academic discussions to an atmosphere of comfort and bliss, their presence has been the prime factor to boost my performance. I also thank other members of DCS, IISER Mohali for continually supporting me and helping me with ideas that strengthen my foundations in this subject.

Finally, IISER Mohali for providing undergraduates a chance to pursue excellent research careers through fantastic laboratory equipment and facilities. Last but not the least, I thank the DST, Government of India for the Inspire Fellowship that has helped in covering a large part of my academic expenses for my undergraduate studies.

List of figures

List of tables

List of abbreviations

IR	Infrared
UV	Ultraviolet
H_2O	Water molecule
Ppf	Propofol
HF	Hartree-Fock
DFT	Density Functional Theory
CI	Configuration Interaction
CC	Coupled Cluster
B3LYP	3 parameters used in the Becke-Lee-Yang Parr functional
M06	Minnesota functional
MP2	Møller–Plesset 2 perturbation theory
ZPE	Zero Point Vibrational Energy
BSSE	Basis set superposition error
AIM	Atoms in molecules method
CP	Critical Point
LMOEDA	Localized Molecular Orbital Energy Decomposition Analysis\
NBO	Natural Bond Orbital

Contents

Abstract

Propofol or 2,6-diisopropylphenol is a popular intravenous anaesthetic that is known to manifest anaesthetic properties by docking onto the tryptophan and the tyrosine residues of the $GABA_A$ receptor. Several x-ray crystallography studies have indicated that the docking mechanism involves hydrogen bonding interactions, exhibited between the hydroxyl groups in propofol and the amino acids involved in the interactions. Moreover, the molecule exhibits several conformations due to the rotational degree of freedom of the isopropyl group with respect to the phenyl ring. The conformational analysis and the study of weak interactions of this biologically significant molecule has been one of the aspects of this study.

Matrix isolation infrared spectroscopy, which has been shown to be a powerful tool to study weak interactions and conformers has been used in the present study together with *ab initio* computations. In this matrix isolation technique, molecules of interest are trapped in an inert host matrix at cryogenic temperatures at high dilutions to ensure isolation. The technique results in spectra that have sharp features enabling one to resolve features due to conformers and complexes formed due to weak hydrogen bonded interactions.

In order to corroborate experimental data, computations were also performed. Geometry optimization algorithms, harmonic analysis and frequency calculations are critical to the understanding of experimental data. Calculations employing various levels of theory such as the B3LYP, M06-2X and MP2 together with 6-311++g(d,p) and the aug-cc-pVDZ basis sets were performed. AIM analysis, LMOEDA and NBO analysis were also performed to understand the nature of interactions that were under consideration.

Conformational analysis yielded five stable conformers computationally, while three were identified in experiments. Earlier work in the literature had not clearly resolved the conformers and our work is, to the best of our knowledge, the first report of conformer resolution in propofol. Fourteen 1:1 hydrogen bonded complexes of propofol with H_2O were obtained computationally, of which the global minimum structure was identified in the matrix. Evidence for the hydrogen bonded complex was obtained from the shifts in the stretching frequency of the O-H group of phenol in propofol. The experimental results were corroborated by computations. Propofol interaction with water presented a rich and diverse landscape of hydrogen bonded isomers, and the work is clearly important as it sheds light on the non-covalent interactions that leads to its biological activity.

Chapter 1

Introduction

1.1 Propofol – The anaesthetic

Propofol or 2,6-diisopropylphenol is a commonly administered anesthetic which has largely replaced other anesthetics, such as sodium thiopental, for surgical and other medical procedures.[1] Propofol has several advantages as an anesthetic, as it is known to undergo complete metabolism, is non nauseating and has a relatively short recovery time for patients who undergo the administration of the drug. The few minor side effects that accompany the drug administration include apnea, blood pressure reduction and exploitation of the drug as a recreational hallucinogenic.[2-3] Though there are no concrete evidences that show the effects of long term damage due to continual use of propofol, the molecule was sensationalized in the year 2011 as an addictive hallucinogenic following the abuse of propofol by the late popular music icon Michael Jackson.[4]

Propofol is mostly marketed as a TIVA (Total Intravenous Anesthesia) and is popularily known by the brand name “Diprivan”. It is nicknamed as the “milk of amnesia” because it is marketed as a white formulation and is a fast acting anesthetic. The formulation is essentially an emulsion of propofol in soya oil and H_2O along with other excipients.[5] The marketing emulsions vary from brand to brand but the original tested emulsion for Propofol was developed by Imperial Chemical Industries as ICI 35868 and was based on the surfactant Cremophor EL formulation[6-7]. Since then the emulsion has undergone significant changes in the concentrations of different additives, mainly aiming to reduce side effects and the pain caused to the area where the anesthetic is administered intravenously.

1.2 Structure and mechanism of action of propofol

Propofol, or 2,6-diisopropylphenol contains the phenolic hydroxyl group in the plane of the phenyl ring and is located between the two isopropyl groups on the 2 and 6 carbon atom of the phenyl ring. The isopropyl groups are attached to the aromatic ring with a C-C single bond which has a rotational degree of freedom. The rotation about the single bond results in multiple geometrical conformations of the molecule, with rather small barriers for conformer interconversion.[8] The center of chemical activity for the molecule is the hydroxy

group, whose chemical activity tends to be modified the adjacent bulky isopropyl groups. [9-11] Moreover a greater degree of complexity is added to the problem owing to the different stable conformations of the molecule, thus allowing various possible combinations in which the phenolic hydroxy group can interact with other moieties and chemically active groups.

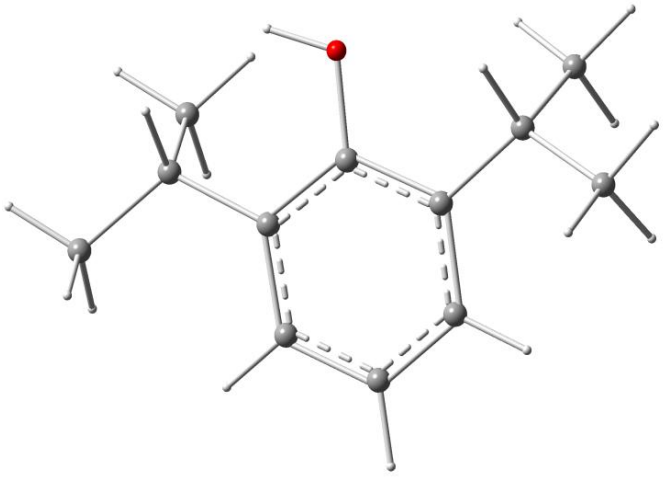

Fig. 1.1: Propofol molecule

It is known from the literature that this molecule docks onto the $GABA_A$ receptor and thus stops the docking of the neurotransmitter GABA. Thereby, acting as an agonist and delaying the closing of the ion channel. This leads to the interruption of the electrical signals between the neurons and thereby results in the anesthetic properties of the molecule. The molecule is carried by the plasma fluid throughout the central nervous system and therefore is quick in action. The molecule is known to dock onto the Tyrosine and the Threonine amino acid residues of the $GABA_A$ receptor, which are known to contain hydroxy groups and x-ray crystallography studies prove that the hydroxy groups are involved actively in the docking mechanism of propofol[12]. Fernandez et. al. have extensively researched the mechanism of hydrogen bonding of the molecule with H_2O clusters, phenol (Tyrosine mimic) and isopropanol (Threonine mimic). Their results, based on spectroscopic techniques like REMPI, UV-IR laser based spectroscopy and mass spectrometry, conclusively corroborate the interaction of propofol with such systems.[13-15] In this work, we plan to undertake the study of the conformations of propofol and its interaction with H_2O, using matrix isolation infrared spectroscopy.

1.3 Hydrogen bonding and weak interactions:

Hydrogen bonding is perhaps the most important form of non-covalent chemical interaction that governs innumerable chemical and biological phenomena. Right from holding the strands of DNA together to protein structure, hydrogen bonds are considered to be the key chemical interactions that govern life form and functions.[16] A hydrogen bond can be viewed as a strong electrostatic interaction between two dipoles. In the classical definition it was restricted to be an interaction of a hydrogen atom attached to a strongly electronegative element in a molecule interacting electrostatically with another electron rich atom through space. However that definition has been constantly modified and in the year 2011, IUPAC formed a committee comprising of eminent scientists who came up with the following definition for the Hydrogen Bond[17]:

"The hydrogen bond is an attractive interaction between a hydrogen atom from a molecule or a molecular fragment X–H in which X is more electronegative than H, and an atom or a group of atoms in the same or a different molecule, in which there is evidence of bond formation."

This definition broadens the criteria needed to classify an interaction as a hydrogen bond. Ideally it is a strong electrostatic and a partially covalent interaction which is weaker than an ionic or a covalent bond lying in the range of 0.2-40 kJ/mol. It has contributions from electrostatic interactions, polarization effects, van der Waal's interactions and also covalence. Moreover when a hydrogen bond is formed in the X-H....Y fashion, where X is an electronegative element, H is the hydrogen atom covalently attached to X and Y is another electronegative fragment, there is a decrease in the stretching frequency of the X-H covalent bond. This is termed as a red shift of the stretching frequency.[18] This shift is crucial for our studies in analyzing hydrogen bonded complexes. There is a partial electron density transfer from the proton acceptor's excess electron density to the proton donor's sigma antibonding orbital.[19] This results in the weakening and the elongation of the X-H bond and therefore is reflected in the red shift of the stretching frequency of the system.

There are also situations when the X-H bond is compressed rather than elongated. Such a situation is termed as improper hydrogen bonding. This notion was introduced in 1998 with the blue shift phenomenon seen in benzene dimers and other such complexes where the C-H stretching frequencies showed a blue shift.[20] Other notions for the hydrogen bonding include dihydrogen bond[21-23], H-π interactions and monoelectron dihydrogen interactions. Thus the concept of hydrogen bonding rather encapsulates a large variety of interactions and it has been an area of immense interest and research.

1.4 Methodology

Every molecular system has a definite energy coordinate for different geometrical positions on its potential energy surface. Using *ab initio* computations we can optimize the geometrical orientations of the molecule based on energy minimization algorithms of suite programs like Gaussian09.[24] These algorithms help us to essentially analyze the features of the surface which is to locate features like maxima, minima and saddle points of different orders. Following geometry optimization, the suite program can calculate the second order Taylor's expansion terms of the energy with respect to the geometrical coordinates. This can essentially help one to calculate the frequencies of the various normal modes that are possible in the configuration of interest. One can also resort to wavefunction based computational methods that can also be used to analyze and understand the system and approach the problem with an independent dimension.

Our experiments were done using Matrix Isolation Infrared Spectroscopy. It is a low temperature isolation technique where we trap the molecules of interest in configurations that correspond to different minima on the ground state potential energy surface of the system. The molecules are trapped in an inert matrix at cryogenic temperatures. The experiments are done in vacuum where the pressure is maintained at 10^{-6} torr or lower. Furthermore, the molecules are taken diluted in a large excess of an inert gas, so that they trapped in the matrix isolated from each other, with very little chance of dimer formation or higher aggregations. Following deposition, an infrared spectrum of the isolated species is then recorded. The inert host matrix is transparent to the infrared radiation. It is therefore possible to isolate conformers, analyze weakly bounded complexes in these experiments.

In order to corroborate our results, our *ab initio* computations are performed, to identify minima on the potential energy surface. Frequency calculations are then done to characterize the nature of the stationary point and also to assign experimental features. This is an effective tool to trap and comprehend the different geometrical conformations of propofol. Different conformers ideally differ in configurations and energies, and vibrational frequencies. In the case of weak hydrogen bonded complexes, the shifts in the monomer's frequencies of normal mode reflect upon the extent of hydrogen bonding between the two fragments that are involved. Our central theme therefore remains the analysis of the conformational aspects of propofol and studies of weak interaction of the molecule with H_2O using Matrix Isolated Infrared Spectroscopy and *ab initio* computations.

Chapter 2

Experimental setup, techniques and procedures

2.1 Matrix Isolation

The experimental technique adopted in this work is Matrix Isolation infrared spectroscopy. The technique consists of preparing an inert host matrix, where the molecules of interest are trapped and studied using a variety of spectroscopic tools. Matrix host materials are usually chemically unreactive gases, such as He, Xe, Ar, Ne and N_2. In order to condense these gases to a solid matrix, one needs a cryogenic setup that works at temperatures in the of the order of a few Kelvins.[25]

The history of such studies dates back to the 1920's and 30's, when low temperature research groups started exploring the domains of cold molecules. However, the technique of Matrix Isolation was independently popularized by Pimentel and Broida in the 1950's.[26,27] With the availability of better cryogenic technologies, the technique gained popularity and importance. Matrix isolation requires high vacuum systems both to maintain the cryogenic temperatures and also to essentially eliminate impurities in the condensed matrix. Thus the basis of the technique therefore rests on two technologies.

a) Cryogenics
b) High Vacuum Systems

The next step in the matrix isolation experiments is the method of analysis of the trapped host inside the solid matrix.[28] Several techniques and probes can be used for the experimental detection and analysis of the host species. ESR, UV-Absorption, FTIR etc. are a few popular methods of chemical analysis for matrix isolated species. With the development of novel instrumental setups, modifications of existing techniques can be designed for advanced and improved analysis of matrix isolated species.

2.2 The nature of the matrix

Usually the cold substrate where one deposits the matrix is at a temperature below one third of the melting point of the host gas, to ensure that the matrix is uniform and rigid. Overall the matrix maybe assumed to be a microcrystalline inert material where diffusion is

prohibited. The matrix may be considered to be crystalline with grain boundaries, which are regions of defects. The regions of defects, voids and interstitial sites serve as usual traps for the molecules of interest. As a result of these defects, site effects come into play and play a critical role in the analysis of isolated species. Noble gases such as Ar freeze in a FCC lattice whereas N_2 freezes in a HCP lattice.[29]

Any matrix needs to satisfy two important criteria, which are chemical inertness and transparency of the matrix to the probe for analysis. The matrix must cause minimal chemical perturbation to the sample of interest. Transparency is a very important criterion that the matrix has to fulfil, so that a clear spectral window is available for the analysis of the sample. Hydrocarbon matrices are therefore unsuitable for infrared studies, as they have strong absorptions in the mid-infrared regions, leaving a very small workable window. However, the same matrix is an excellent matrix material for fluorescence studies as these matrices do not show any fluorescence on excitation with visible or ultraviolet light. Hence a matrix suitable for one spectral region may be unsuitable for another and a judicious choice must therefore be exercised. [28]

2.3 Matrix isolated species

Typically for matrix isolation experiments the matrix: sample ratios are kept in the realm of 1000:1. Such dilutions ensure isolation of the host with a negligible population of the dimers or higher clusters. The presence of higher clusters leads to complications in the spectral assignments as spectral features and the spectra is complex and tough to comprehend. It can be shown from probability analysis that for small molecules, matrix to sample ratios of 1000:1 ensure about 99% of isolation of the samples to be analysed.[28,30]

2.4 Analysis of matrix isolated species

Since temperatures much lower the melting points of the matrix gas are employed, it is valid to assume that the matrix is immobile and devoid of any diffusion processes. As discussed earlier, it may also be assumed that under proper conditions, the species in the matrix are well isolated. We can then analyse the species of interest, using any of the spectroscopic methods such as UV-visible absorption, IR, ESR, and fluorescence, depending on the information sought in the study. The diffusion process in the matrix is temperature dependent and is given by the following relation;

$$\textbf{Rate} \propto \mathbf{e}^{(-\Delta E/RT)}$$

At temperatures approaching half the melting point, significant diffusion of the trapped processes occurs[28]. This onset of diffusion can be used to advantage, by promoting the aggregation of the trapped species to study intermolecular interactions between them. These interactions are usually manifested as unique spectral features, often very different from that of the monomeric species. This process of warming the matrix to deliberately promote diffusion is known as *annealing* and is a standard technique employed to study weak interactions. The warmed matrix is held at this elevated temperature for a certain period of time (~30-60 minutes) after which it is cooled to the original low temperature. A spectrum of the matrix thus annealed is again recorded to identify the features of the adducts formed.[31]

2.5 Matrix Isolated Fourier Transformed Infrared Spectroscopy (MI-FTIR)

2.5.1 Theory

The combination of the Matrix Isolation setup with an FTIR Spectrophotometer is probably the most popular technique that has been employed for the study of cold isolated molecules. The infrared spectrum of a molecule is the vibrational fingerprint of a particular species. In the case of gas phase IR spectrum of a molecule, one observes both vibrational as well as the rotational lines of the species of interest, with molecules populating a large number of rotational levels. Consequently, a large number of lines or a broad profile is often observed. Moreover, at higher temperatures the infrared lines of analyte molecule are broadened due to Doppler and Collisional broadening. At cryogenic temperatures, both Doppler and Collisional broadening are suppressed with molecules frozen into the ground rovibronic state.[32] This collapses the peak to extremely sharp lines corresponding only to rovibrational transitions from the lowest vibrational and rotational levels. However, to derive the advantage of small linewidths at cryogenic temperatures molecules, it is essential that the molecules in question are not allowed to aggregate and hence the need for isolation. To ensure isolation one needs to trap the species of interest in a host matrix as described in detail earlier.

However, matrix isolation spectra are not as simple as described above, as site effects and matrix interaction can often complicate the spectra. Though the matrix is chemically inert, nevertheless they do manifest subtle influences which are reflected as shifts in the infrared frequencies compared with gas phase data or as multiplets in spectral structure. Care has therefore to be exercised in the analysis of spectra to ensure that these effects are

appropriately considered in the analysis. .

Shifts in frequency in the matrix relative to gas phase values arise mainly due to four major factors:

1) Electrostatic - ($\Delta\upsilon_{elec}$)
2) Inductive - ($\Delta\upsilon_{ind}$)
3) Dispersive - ($\Delta\upsilon_{dis}$)
4) Repulsive - ($\Delta\upsilon_{rep}$)

$$\Delta\upsilon = (\upsilon_{matrix} - \upsilon_{gas}) = \Delta\upsilon_{elec} + \Delta\upsilon_{ind} + \Delta\upsilon_{dis} + \Delta\upsilon_{rep} \quad ....(1)$$

Where υ_{matrix} is the frequency of a given mode of a sample in matrix and υ_{gas} is the frequency of the same sample molecule in the isolated gas phase. As discussed before, site effects do contribute to changes in the spectroscopic information and vary from host material to material due to the differences in the $\Delta\upsilon_{dis}$ and $\Delta\upsilon_{rep}$. We expect the matrix to weakly interact with the analyte molecules hence the contributions from $\Delta\upsilon_{elec}$ and $\Delta\upsilon_{ind}$ are assumed to be minimal. The choices of matrix materials for our experiments thus are restricted to inert gases like Ar and N_2.

As discussed before, matrix host gases crystallize in different lattices with differing lattice parameters. Hence the environment experienced by the host differs depending on the matrix. Theoretically it has been shown that tighter cages result in blue shifts[33] and loose cages lead to red shifts in the vibrational frequencies of the analyte.[26] This is explained by the Buckingham model[34], to analyse the perturbation on the frequency of the analyte due to solvent effects. This model applied to inert gas cages reduces to

$$\Delta\upsilon = (\upsilon_{matrix} - \upsilon_{gas}) \sim (\upsilon_{matrix} - \upsilon_{gas}) = (B_e/hc\omega_e)(U'' - 3AU'/\omega_e) \quad ....(2)$$

Here,

$B_e = h/8\pi^2 c\mu r_e^2$ is the rotational constant,

a = Anharmonicity constant,

U = Energy due to solute-solvent interaction,

$U' = \{\partial U/\partial r_{BC}\}$ and $U'' = \{\partial^2 U/\partial^2 r_{BC}\}$,

$c\omega_e$ = Harmonic oscillator frequency

The Buckingham expression can essentially help us to rationalize the frequency shifts that occur in a matrix relative to gas phase values. The following potential energy diagram explains the frequency shifts that occur inside the matrix due to the interaction of the host matrix with the analyte.

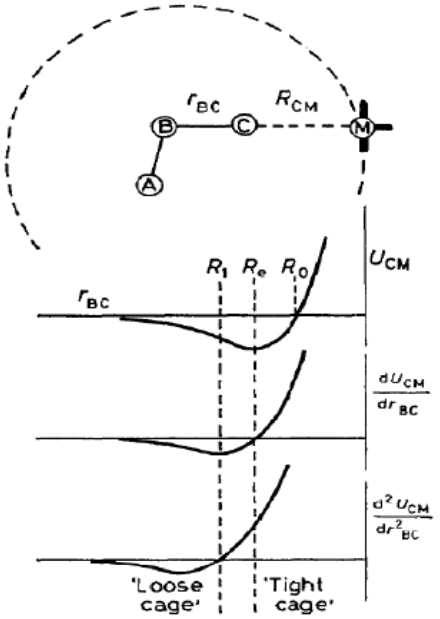

Fig. 2.1: Cage effects and frequency shifts for the sample molecule [25]

One can refer to **Fig 2.1** and recognize that if the cage is very tightly packed; i.e. for small distances between the host and the guest, the U'' term in equation 2, is positive, the shift seen in this case is positive (a blue shift). On the other hand, for large distances between the host and the guest, which is the equivalent of a loose cage, the observed shift is negative (i.e. a red shift). Thus matrix can induce pronounced but subtle effects which one needs to take specific care of in the analysis of spectra. In addition to the matrix effects, several other possible phenomena mentioned below, result in the variation of the matrix isolated spectrum with respect to the gas phase spectrum of the molecule.

These include the following:

1) Rotation of the solute molecules in its trapping site,
2) Multiple trapping site effects,
3) Aggregation of the solute,
4) Lifting of degeneracy of the vibrational levels,
5) Induction of inactive modes by the matrix. [35,36]

The detailed discussion on the mentioned above effects is discussed in the literature. Thus, while matrix isolation offers an excellent tool to study cold isolated molecules, it also throws up enough challenges in the analysis of the spectra due to all the factors mentioned and discussed above. Our, interests in this work, is to employ matrix isolation infrared

spectroscopy to study the conformations of Propofol. In addition, we have also studied the weak non-covalent interactions between propofol and H_2O, specifically addressing the study of the 1:1 hydrogen bonded complexes. Matrix isolation clearly is an efficient technique for these studies.

2.5.2 Instrumentation

The matrix isolation- FTIR setup is essentially composed of the following units:

2.5.2.a. *FTIR Spectrophotometer*

2.5.2.b. *The cryostat and its associated units*

2.5.2.c. *The vacuum systems*

2.5.2.d. *Sample Chambers and Deposition Units*

2.5.2.a. FTIR Spectrophotometer:

An FTIR Spectrophotometer works by the excitation of the vibrational modes of a molecule by shining infrared light on the sample. The sample to be analysed is usually loaded onto a substrate, such as KBr, which is transparent to the wavelength of light used. The common practices of obtaining an infrared spectrum of a sample include methods like liquid film, sample in KBr pellet, Attenuated Total Reflection (ATR) and diffuse reflectance (DRIFT). The incident beam is directed on the sample which absorbs specific wavelengths in the beam, which correspond to the frequencies of the IR active normal modes of the molecule. The resultant transmitted beam is then directed onto a detection unit which is then Fourier-Transformed to yield the IR spectrum of the sample.[37] The data can then be acquired for further analysis. The general instrumental layout for an FTIR Spectrophotometer shown in **Fig. 2.2**, which works on the principle of a Michelson interferometer:

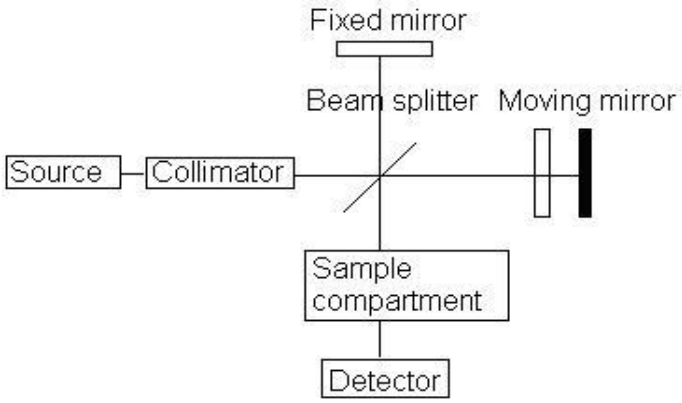

Fig. 2.2: The schematic diagram of an FTIR spectrophotometer (www.mit.edu)

The matrix isolated molecules are studied in these experiments using a Bruker-Tensor 27 FTIR Spectrophotometer. The instrument was operated at a resolution of analysis fixed at 0.50 cm^{-1}. In all the experiments multiple scans (n= 8-16) were recorded to obtain a spectra with a good signal to noise ratio, as the S:N ratio improves with the square root of the number of scans. The wavelength of operation was set over a range of 4000-400 cm^{-1}. [38] In the case of matrix isolated experiments the incident light is made to pass through KBr window mounted on the cryostat tip. On this substrate the matrix with the sample was deposited for eventually recording the spectra.

2.5.2.b. Cryostat

The heart of the technique is in the cryogenic system that provides the cryogenic temperatures for the deposition of a matrix. Commercially, several low temperature micro refrigerators using Nitrogen, Hydrogen and Helium as working fluids are available which can attain temperatures of 77K, 20K and 10K respectively.[28] The setup used for this work is based on a closed cycle Helium compressor. The cryostat used is a Sumitomo closed cycle Helium compressor (HC-4E1) that uses expansion-compression cycle of Helium for cooling[39]. It is to be noted that it is the tip of the cryostat, known as the expander or the cold finger (also addressed as the cryo-tip) that attains a temperature of around 10K. The closed cycle cryostat used in our setup works on the Gifford McMahon Cycle and it is this expander where this Gifford McMahon refrigeration takes place. The connections to the cryostat from the compressor are done through two gas lines for the working fluid and a cable for electrical supply. The inlet pipe allows the high pressure Helium into the cryostat whereas the outlet pipe allows the low pressure gas to flow out, controlled by the cryostat.[40]

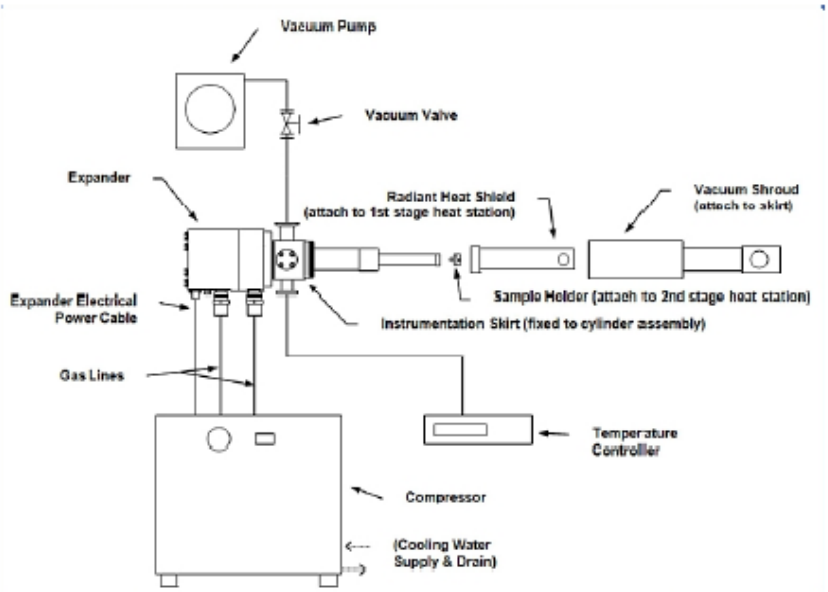

Fig. 2.3: The general schematic for the cryosystem assembly

Grifford Mcmahon Refrigeration Cycle: The rotation of the valve disk opens and allows the high pressure He gas to pass through the regenerating material into an expansion process. The difference in pressure drives the piston upwards allowing the gas at the bottom to expand and cool. Consequently, the rotation of the valve disk then opens the low pressure path allowing the cold gas to flow through the regenerating material. This results in the heat extraction process, and the cooling is the consequent result for this cycle. Finally the pressure differential returns the displacer to its original position completing the cycle.

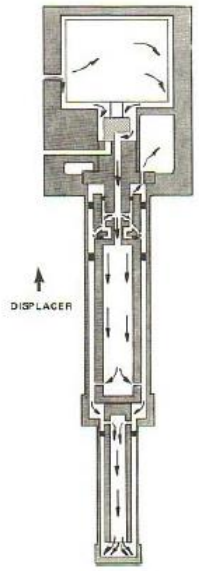

Fig. 2.4: The movement of the high pressure He gas through the regenerating material

A vacuum shroud is provided, which shields the cold end of the expander under vacuum. The heat load on the expander caused by conduction and convection are limited by this shroud. The radiation shield, actively cooled by the first stage of the expander, insulates the second stage from the thermal radiation being emitted from the vacuum shroud. The setup comes with external support systems handling the electrical components associated with the setup. An instrumentation skirt is also provided along with this setup which contains vacuum and electrical ports. The region of the cryostat tip is maintained at high vacuum conditions and is a part of the advanced cryogenics which are necessary for such experiments. The cryostat is maintained at a temperature of 12K while recording the spectra and increased to 30K (N_2) for the annealing process, as previously described, for a period of 30-60 minutes. The temperature changes are controlled using an electronically controlled temperature controller unit (Lakeshore Instruments). The compressor is cooled by 3kW water chiller system (Werner Finley) that maintains flowing water at an approximate temperature of 17°C.

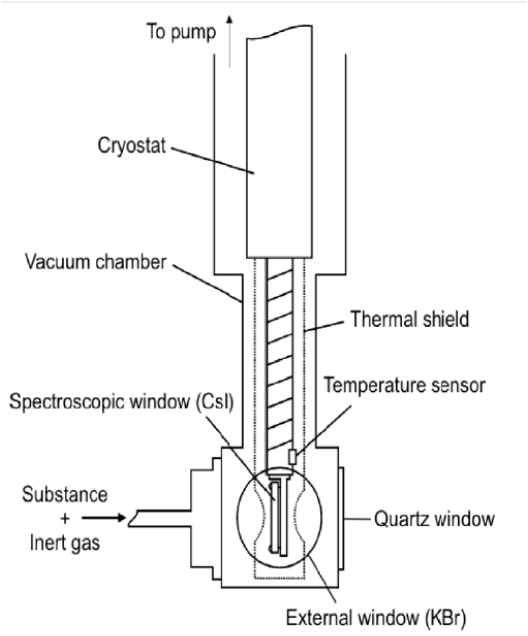

Fig. 2.5: The schematic for the cryostat head mounted on the FTIR Spectrophotometer

Fig. 2.6: (From L-R) a) The cryostat b) The He Compressor c) Temperature control unit

2.5.2.c. Vacuum system

The setup needs to function under high vacuum conditions (better than 10^{-6} torr) for obtaining spectra devoid of any impurities. This requires for the setup to reach pressures as low as possible to reduce impurity bands. The vacuum thus obtained in this setup is attained in two steps. Firstly by a mechanical rotary pump (Hind Hivac; ED6) operating at a pumping speed of 200 L/min followed by a vapour diffusion pump (Edwards, Diffstak MK2 series 100/300) operating at a pumping speed of 300L/sec. Working of diffusion pump is based on momentum transfer to gas molecules from a directed jet of oil. Vapour is conducted upward through a tower above the boiler to an array of fine nozzles from which the vapour is emitted in a jet directed downward and outward toward the pump walls. The diffusion pump walls are usually water-cooled so that molecules of the working-fluid vapour condense before their motion is randomized by repeated collisions. The walls of the diffusion pump are cooled by water from a chiller (Werner-Finley). The diffusion pump requires to be backed by the rotary pump, and the two pumps together achieve an ultimate pressure of ~1 x 10^{-6} torr.[28]

The vacuum is measured using a digital Penning gauge (Hind Hivac) and a Pirani Gauge 26 (Edwards APG 100 Active Pirani Gauge).

Fig. 2.7: (L-R) Diffusion pump, Penning Gauge and Pirani Gauge

2.5.2.d. Sample chambers and deposition techniques

The matrix host gas and the sample of interest are usually mixed and allowed to equilibrate in a sample chamber. The sample chamber is a 1L stainless steel cylindrical chamber with a number of ports for sample introduction and pumping. As mentioned earlier, one uses a matrix to sample ratio of 1:1000.[28]

The sample gas is first admitted to the chamber first, following which the matrix gas (N_2 or Ar) is filled into the chamber to the desired pressure. This is followed by an equilibration step, which allows the gas to equilibrate for a period of not less than 15 minutes. This ensures proper mixing and then the gas is usually deposited onto the cryostat by streaming the gas mixture from the mixing chamber through a Cu tube, the flow being adjusted by using needle valve that controls the outflow of the gas. The deposition rate is usually maintained at ~3mmol/hour. This ensures the formation of a matrix that is uniform in nature.

The concentration of the sample in the mixing chamber is usually controlled by maintaining the vapour pressure over the sample at a desired value, by maintaining the sample at the appropriate temperature. The temperature of the sample is controlled using an ethanol-liquid nitrogen slush bath. The temperature of the bath is monitored using a platinum resistance thermometer. In some experiments, a double jet assembly is used, where the sample was streamed through one nozzle, while the matrix gas was allowed to stream through a second nozzle. All the experiments with propofol were conducted using the double jet assembly. The low vapour pressure of propofol (vapour pressure of 5.6 mm of Hg at 100°C) precluded the use of a single jet assembly.

Fig. 2.8: (Clockwise from top left): a) The mixing chamber; b) Sample chamber & mixing chamber; c) The needle valve; d) The double jet setup mounted on the cryostat

Fig. 2.9: The MI-FTIR setup

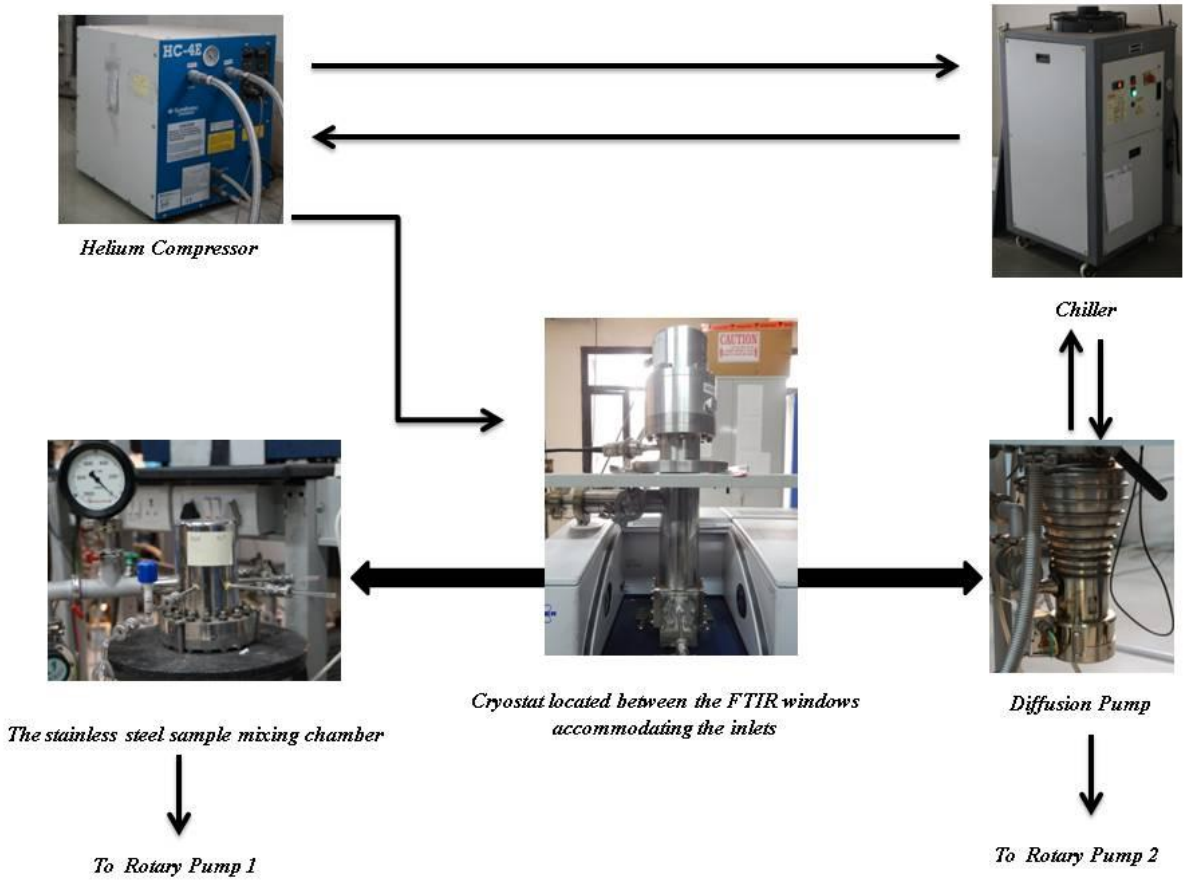

Fig. 2.10: The schematic of the MI-FTIR setup.

Chapter 3

Computational Methods

3.1 History and developments in Computational Chemistry

Chemical properties of atomic and molecular systems can be extensively simulated using computers. Computational Chemistry started developing under the lights of Theoretical Chemistry and Chemical Physics. With the development of the Quantum Theory in the 1920's, calculations of several molecular and atomic properties were possible. These calculated properties provided significant insight into the working of several experiments performed in the laboratory.

A breakthrough in this field came with the development of the Hartree-Fock equations in the year 1930. The history of *ab initio* computations lies in the implementation of the Hartree-Fock equations into computer programs. James and Coolidge published their first set of quantum mechanical calculations on the H_2 molecule in the year 1933.[41] In 1950 Boys introduced Gaussian-type basis functions for simulating orbitals and in the following year the foundations of computational chemistry were laid by the development of the matrix version of HF method by Roothaan and his co-workers. Roothaan's equations are the backbone to several algorithms used in different computational suites used for *ab initio* calculations. Quantum mechanics thus paved a path that lead to the foundations of computational Chemistry.[42]

Independently, in the year 1927, Thomas and Fermi developed a theory using statistical mechanics that could relate the electron density on a system with the average energy of the system. The theory remained relatively stagnant for a few decades till the celebrated Hohenberg-Kohn Theorem came into play. The Hohenberg-Kohn-Sham version of the theorem proved to be another breakthrough for computational chemistry. This theory used functionals instead of the quantum mechanical wavefunction picture and was widely celebrated as the Density Functional Theory. DFT calculations can be extended to several large systems because it a method that is known for computational efficiency. It is the most widely used for electronic structure calculations of atoms, molecules, solids, nanomaterials, synthetic materials, biological molecules and surfaces. It was in the year 1998, Walter Kohn was awarded the Nobel Prize in Chemistry for “his development of the density-functional theory.”[42,43]

Molecular properties such as structures, energies, frequencies, dipole moments and electron distribution can be obtained fairly accurately from such calculations. With the advent of better technologies, computational efficiency and smarter algorithms, computational chemistry has gained a thrust and has developed into an independent branch of chemical sciences. Hybrid theories combining DFT and quantum mechanical methods are very popular and have been exploited for analysing our system of interest. Popular methods for analysing molecular systems include Hartree-Fock (HF), Density Functional Approaches (and modifications), Møller Plesset Perturbation Theory (MPn), Configuration Interaction Method (CI), Coupled Cluster (CC), Multi-Configuration Self Consistent Field etc.

3.2 *Ab initio* computations for the propofol system

Propofol or 2,6-diisopropylphenol, our system of interest has been investigated extensively using *ab initio* computations. Insights into molecular parameters such as structures, energy and frequencies of molecular vibrations help us to analyse and corroborate our experimental data. The system has been investigated for conformations and its weak interactions with H_2O. Monomer geometries were optimized using the Gaussian09 suite of programs. The hydrogen bonded complexes between propofol and H_2O were then optimized using the computed monomer geometries. Harmonic vibrational frequency analysis was also performed to ensure that all the optimized structures were minima on the potential energy surface with real positive frequencies. To understand the nature and strength of these non covalent interactions, we performed natural bonding orbital analysis (NBO)[44] using the Gaussian09 suite of programs. Energy decomposition analysis of the system was carried out using the GAMESS [45]suite of programs and to understand the partitioning of interaction energy into various components. Bader's Atoms in Molecules (AIM) analysis was implemented using the AIM2000 suite of programs to locate the Bond Critical points [46].

3.2.1 Basis Sets

Geometry optimizations and frequency calculations were performed using different a*b initio* methods. The calculations were primarily done at the B3LYP, M06-2x and the MP2 levels of theory employing different basis sets. A large number of basis sets are available to a computational chemist and there is a trade off between the size and intricacy of a basis set and the computation time and resource needed. For our calculations the 6-311g++(d,p) and the aug-cc-pVDZ basis sets were employed.The 6-311g++(d,p) basis is a split valence basis set. The *A-BCg* form of basis sets was primarily developed by J. A Pople and his co-workers.

In this case, *A* represents the number of primitive Gaussians comprising each core atomic orbital basis function. The *B* and *C* indicate that the valence orbitals and are composed of two basis functions each, the first one composed of a linear combination of *B* primitive Gaussian functions, the other composed of a linear combination of *C* primitive Gaussian functions. The 6-311g++(d,p) basis set includes diffusion and polarization functions [47]. The aug-cc-pVDZ bais belongs to the family of 'correlation-consistent polarized' basis sets and the 'V' indicates they are valence-only basis sets. They are designed to converge systematically to the complete-basis-set (CBS) limit using empirical extrapolation techniques. The pioneers in developing these basis sets were Dunning and his co-workers.[48]

The methods employed in the computations are described in greater details in the following subsection:

3.2.2 B3LYP (Becke-Lee-Yang-Parr) Method:

B3LYP is an extremely popular DFT method for *ab initio* computations. As described before, all DFT methods employ a functional approach and electronic properties of the system are determined from the electron density. The BLYP is one such functional which also includes some HF exchange. This includes the electron spin densities and their gradients. The most commonly used functional in this category is the B3LYP. The B3LYP includes the Becke three parameter non-local exchanges functional with the non-local correlation of Lee, Yang and Parr.[49]

3.2.3 M06 and related methods

The M06 set of functionals were developed by Truhlar et. al. The Minnesota functionals (M0x) are hybrid DFT methods which are developed keeping Scuseria and Staroverov's six strategies in mind, that have been widely employed for designing density functionals. They include: (1) local spin density approximation (LSDA), (2) density-gradient expansion, (3) constraint satisfaction, (4) modelling the exchange-correlation hole, (5) empirical fits, and (6) mixing Hartree–Fock and approximate DFT exchange.[50] The M06 functionals are set of four meta-hybrid GGA functionals (generalised gradient approximation-it depends on the up and down spin densities and their reduced gradient). The M06-2x method has been widely employed for *ab initio* computations for this system. The 2x is refers to the percentage of HF exchange which roughly amounts to 54% in this case. It is recommended that the M06 functional is applied to problems in organometallic chemistry and noncovalent interactions. The M06 functionals are thus best suited to model dispersion

interactions.[51]

3.2.4 Møller Plesset Perturbation Theory

The methods employing Møller Plesset Perturbation Theory are non DFT methods and work by brute force solutions of quantum mechanical wavefunctions. The main problem with the Hartree-Fock approach is that it cannot account for electron correlation in molecular and atomic systems. However, there exist several methods for treating the electron correlation problem starting from a Hartree-Fock (HF) single determinantal wave function. Configuration interaction (CI), Møller Plesset (MP) (or many-body) perturbation and the coupled cluster (CC) are some of the widely used formalisms to calculate the electron correlation energy. The MP Perturbation Theory was developed in the year 1934 by Christian Møller and Milton S. Plesset. This method essentially treats the electron correlation using the Rayleigh-Schrodinger perturbation theory to second (MP2), third (MP3) and fourth (MP4) order. This was extended to the fifth order (MP5) by Raghavchari et. al., but it must be noted that at higher orders the theory may not necessarily be convergent.[52]

3.3 Geometry optimizations and Frequency calculations

Iterative self consistent algorithms help to optimize a guess geometry into an energetically stable configuration. These algorithms trap critical points on the potential energy surface of the system. The minimum on the surface is the stable geometry in which the molecule may exist. The second derivative of the energy term at the critical point evaluates vibrational frequencies for that particular geometry. For a minimum, all frequencies of vibration should be positive whereas for other critical points like saddle points, there can be imaginary frequencies for one or more modes of vibration.

The energy of the optimized structure is the energy that the suite calculates for the configuration at the optimized geometry. However, while studying weak chemical interactions between two species of interest; one needs to calculate whether the interaction results in stability. Structure can be judged by computing the interaction energy as,

$$\Delta E = E_{complex} - (E_{monomer\ 1} + E_{monomer\ 2})$$

$E_{complex}$ = Energy obtained after the interacting systems have been optimized to a minimum

$E_{monomer}$= The raw energies of the monomers optimized to a minimum (independently)

If ΔE is a negative value, this implies the interaction between the two species leads to stability and together they exist as a stable complex. However, the interaction energy

calculated above, referred to as uncorrected energy, is not sufficient for understanding interaction between two species. Even at absolute zero, molecules are in a state of vibration in v=0. The zero point point energy is $0.5\Sigma h\nu$, where ν is the frequency of a given normal mode of vibration and *h* is the Planck's constant. The interaction energy must therefore be corrected for zero point correction, and is referred to as zero point corrected interaction energy.

Another important correction in energy that has to be implemented in this scheme is the Basis Set Stabilisation Energy correction, abbreviated as BSSE correction to the raw stabilisation energy. This arises due to difference in the number of basis functions used for calculating the $E_{complex}$ in comparison to the number of basis functions used for computing the values of the $E_{monomer}$. When the energy of complex ($E_{complex}$) is computed, the basis functions used are those of both the monomers combined together, while for computing the energy of the individual precursors (i.e. $E_{monomer}$), the basis functions only corresponds to that of the precursors used. As the number of basis functions becomes larger in the computation of the complex, the energy obtained will be lower, due to the fact that each monomer can now use the basis functions of other. This leads to an overestimation of energy in the error being termed as BSSE. The best way to eliminate the BSSE is to increase the basis set until the stabilization energy is the desired minimum, but with a tradeoff of large computation times for even small systems. However, a shorter and a more elegant approach to this problem is to use the counterpoise correction as proposed by Boy's and Bernadi. In this scheme, the energies of both monomers and the complex are computed using the basis used for the complex. Hobza and Havlas have elegantly described the scheme of counterpoise-corrected PES's of H-bonded systems.[53] The scheme of counterpoised BSSE correction be mathematically expressed as the following:

$$.E = E_{Complex}\,(Complex\ Basis) - \{E_{Monomer\ 1}\,(Complex\ Basis) + E_{Monomer\ 2}\,(Complex\ Basis)\}$$

Stabilization Energy is corrected individually for ZPE and BSSE, as applying BSSE correction over the ZPE corrected energies leads to overestimation of interaction energy involved in the question.

3.4 Atoms-in-molecules (AIM) methodology

The atoms in molecules theory is a method to observe the topology of electron density in space locate bond paths and define bond critical points for a system. The method was

developed by Bader and his co-workers. The first step in the AIM analysis is to obtain a wavefunction file from an optimized geometry of the system. This can be done using a suite program like Gaussian09. This wavefunction output file is used as the input to the AIM2000 software which can essentially develop the electron density plot from the generated wavefunction of the optimized geometry. From the electron density plot one can obtain the bond critical points, charge density $\rho(r)$, Laplacian of charge density $\nabla^2\rho$, which is also the trace of the Hessian matrix of $\rho(r_c)$. The charge density is a quantity that can be considered as the distribution of electrons in space. The topology of the charge density is what decides the bonds between two atoms. One can define the critical points of $\rho(r_c)$ as the points where the derivative of the function vanishes. The nature of the critical points is defined using the rank and the signature of the Hessian matrix. The rank of critical point, denoted by ω, is equal to the number of non-zero eigenvalues or non-zero curvature of ρ at the critical point. The signature denoted by σ, is the algebraic sum of the signs of the eigenvalues. The critical point (CP) is labelled by giving the values (ω, σ). A (3, -1) CP corresponds to a bond between two atoms, a (3, +1) CP to a ring, a (3, +3) CP to a cage and a (3, -3) CP corresponds to a maximum. The numbers of critical points of all types, which can coexist in a system with a finite number of nuclei, are governed by the Poincare-Hopf relationship.

$$n - b + r - c = 1$$

Where, n is the number of nuclei, b is the number of bond critical points, r is the number of ring critical points and c is the number of cage critical points.

The sum of three Hessian eigenvalues (λ_1, λ_2, λ_3) at a bond critical point is the quantity $\nabla^2\rho$ or the Laplacian of the charge density. It provides a useful characterization of the electronic charge density distributed in the internuclear region. If the value of charge density ρ ($<10^{-1}$ a.u.) and the curvature of charge density are large, Laplacian of charge density may be positive or negative and is usually in the same order of magnitude as $\rho(r_c)$, then the interaction is of shared type, typical of covalent interaction. For the closed shell interactions, such as hydrogen bonded complexes, van der Waals complexes and ionic systems, the charge density ρ ($\sim10^{-2}$ to 10^{-3} au) at the bond critical point is quite small and the Laplacian of the charge density is positive.[54]

3.5 Energy Decomposition Analysis

LMOEDA is used to identify the physical origin of the total energy based on the inter/intramolecular interactions in a complex. When a complex is formed between two monomers it is important to classify the kind of interactions under consideration. LMOEDA

partitions the components of total interaction energy in terms of electrostatic energy, exchange energy, repulsion energy, polarization energy, and dispersion energy in a complex.[55] EDA helps us to understand the nature of interactions that govern the ultimate stability of a formed complex, for example hydrogen bonded interactions are primarily composed of electrostatic interactions, and EDA plays a crucial role in understanding such interactions. LMOEDA was performed on the GAMESS suite of programs using optimized geometries from G09 output files.

3.6 Natural Bond Analysis (NBO)

NBO Analysis is performed for complexes in order to understand the role of delocalization interactions in the stability of the complexes. Second-order perturbation energies of the various donor−acceptor orbital interactions can be computed as per the NBO analysis scheme. These orbital interaction energies are a function of both the energy difference between the donor and acceptor orbitals and their overlap. These calculations provide information on the orbital delocalizations responsible for the stability of a structure. Like the LMOEDA, it compliments our understanding of the weak interactions.[44]

3.7 Summary

Computations allow us to explore and corroborate our experimental data providing us with useful insight for understanding various molecular systems. In the age of interdisciplinary sciences computation and theoretical modelling of experiments form the backbone for many scientific disciplines. The theoretical data and the experimental results of Matrix Isolation FTIR experiments help in exploring several interesting phenomena in the propofol molecule. The conformational analysis and the weak interaction studies of the system with H_2O have been discussed in the subsequent chapters.

Chapter 4

Conformational Analysis of Propofol

Propofol or 2,6-diisopropylphenol is known to manifest several molecular conformations. The two isopropyl groups, attached to the aromatic ring through a C-C single bond have rotational degrees of freedom, which give rise to multiple geometrical conformations of the molecule.[8] In this work we have explored the ground state potential energy surface of the molecule using *ab initio* computations and have also experimentally examined in detail, the conformers of this molecule using matrix isolation FTIR spectroscopy.

4.1 *Ab initio* computations for geometry optimizations of conformers

Fig. 4.1 indicates the possible rotational degrees of freedom of the isopropyl groups along the C-C bond axis. Lessari et.al and Fernandez et.al.[8,11-15,56] have reported that the system exhibits five stable conformations. Our calculations at various levels of theory and basis sets are in agreement with their findings. The structures for the system were optimized at the B3LYP, M06-2X and the MP2 levels of theory employing the aug-cc-pVDZ and the 6-311++ g(d,p) basis sets.

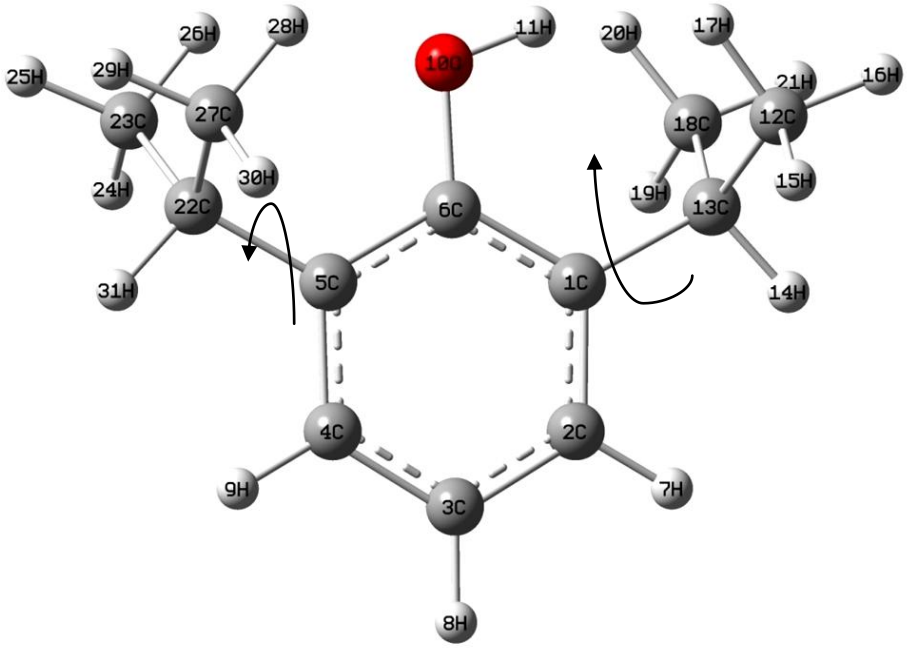

Fig. 4.1: The propofol molecule

The conformations of propofol have been defined in literature with reference to the

orientation of the H atoms with respect to the aromatic ring. It must be noted that the phenyl ring, and the phenolic group lie in the same plane in all the conformers. As seen from the **Fig. 4.1**, H- atoms numbered 31 and 14 are aligned antiperiplanar with respect to the phenolic group; i.e. the hydrogen H14 is the same plane as the phenyl but oriented such that the dihedral angle C6-C1-C13-H14 is ~180^{o}. Likewise, H31 is oriented in the same plane with a dihedral angle C6-C5-C22-H31 of ~180^{o}. This alignment is a stable configuration of the molecule and has been denoted as the EE' conformer. The notation E and E' has been used to indicate the subtle difference between the two hydrogens H14 and H31, as one of them H14, is on the same side of the C6-O10 bond as the phenolic hydrogen, H11, while in E', the hydrogen H31 is oriented away from the phenolic hydrogen with respect to the C6-O10 bond. The other possible stable orientations for the molecule results from the gauche orientation of the H-atom of the isopropyl group with respect to the hydroxyl hydrogen. For the gauche orientation of the isopropyl hydrogens, there are two possible distinct conformations. One isomer is the $G^{\pm}G^{\pm}$ isomer, when both H atoms are on the same side of the aromatic plane. The other gauche conformer, is one where the two hydrogens are on opposite sides of the aromatic plane and is denoted as $G^{\pm}G^{\mp}$ conformer. The other two possibilities include the $G^{\pm}E'$ and the $EG^{\pm}$ conformers. In each case one H atom is eclipsed while the other isopropyl hydrogen is gauche with respect to the O-H group. Hence the five stable conformers are the EE', $G^{\pm}E'$, $EG^{\pm}$, $G^{\pm}G^{\pm}$ and $G^{\pm}G^{\mp}$ conformers.

The geometry optimization procedures using MP2, M06-2X and B3LYP levels of theory employing the 6-311++g(d,p) and aug-cc-pVDZ basis sets indicated that the $G^{\pm}G^{\pm}$ and $G^{\pm}G^{\mp}$ conformers to be almost isoenergetic . Fernandez et. al.[8] also made similar observations and further reported a small barrier for interconversion between the two isoenergetic conformers, at the B3LYP/6-311++g(d,p) level of theory. Our calculations at the MP2/6-311++g(d,p) level agree with their observation.

The MP2/6-311++g(d,p) and B3LYP/6-311++g(d,p) levels indicated the $G^{\pm}G^{\mp}$ conformer to be the most stable conformer; while at the M06-2X/6-311++g(d,p), M06-2X/aug-cc-pVDZ, B3LYP/aug-cc-pVDZ and MP2/ aug-cc-pVDZ levels the $G^{\pm}G^{\pm}$ isomer was indicated to be the lowest in energy. The $EG^{\pm}$, $G^{\pm}E'$ and EE' conformers follow these two low lying conformers in the ascending orders of energy, at all levels of computations. **Fig 4.2** shows the conformers and their relative energy ordering.

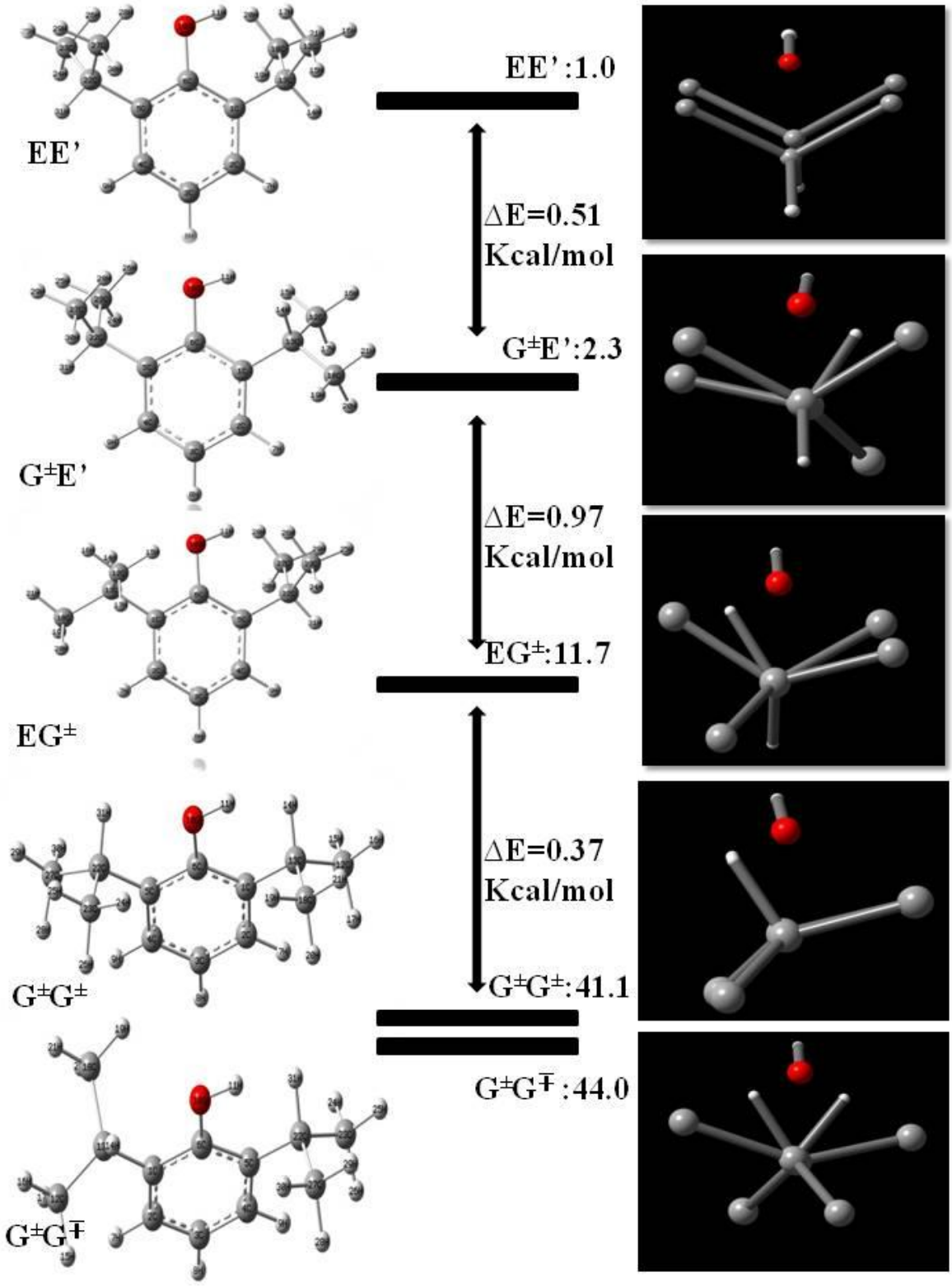

Fig. 4.2: The relative ordering of the conformers with respect to energy. Structures were optimized at the MP2/aug-cc-pVDZ level of theory

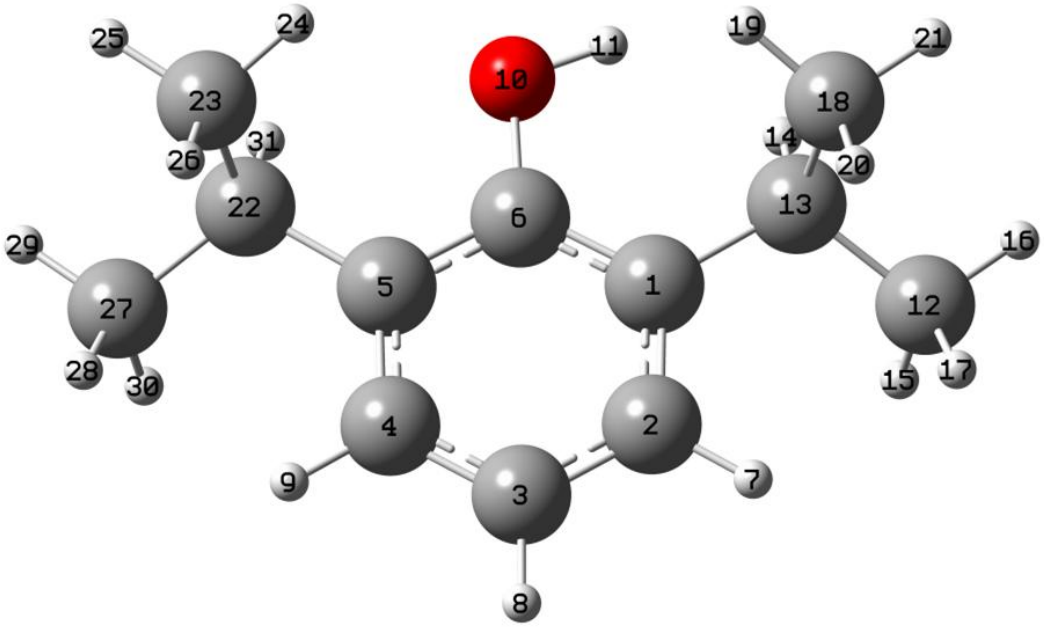

Fig. 4.3: The figure shows the $\mathbf{G^{\pm}G^{\pm}}$ isomer and gives the numbering system for the atom connectivity in the molecule.

Table 4.1: The dihedral angles computed for the different conformers at the MP2/ aug-cc-pVDZ. Refer to **Fig. 4.3** for the dihedral angles in discussion.

Conformers	$\Delta_{14\text{-}13\text{-}1\text{-}6}{}^{\circ}$	$\Delta_{31\text{-}22\text{-}5\text{-}6}{}^{\circ}$
EE'	179.99	-179.99
$\mathbf{G^{\pm}E'}$	179.90	38.61
$\mathbf{EG^{\pm}}$	41.79	179.92
$\mathbf{G^{\pm}G^{\mp}}$	-41.49	-38.79
$\mathbf{G^{\pm}G^{\pm}}$	-41.84	38.93

Table 4.2: Energy ordering the relative (raw) energy with respect to the most stable conformer. Vibrational analysis shows all positive frequencies thus they are considered as stable geometries corresponding to minima on the molecular PES (except at the MP2/-aug-cc-pVDZ level where vibrational analysis was computationally taxing).

Level of Theory	Conformers				
	$G^{\pm}G^{\pm}$	$G^{\pm}G^{\mp}$	$EG^{\pm}$	$G^{\pm}E'$	EE'
B3LYP/6-311++g(d,p)	~0.00	0	0.47	1.03	1.54
B3LYP/aug-cc-pVDZ	0	0.04	0.75	1.23	2.02
M06-2X/6-311++g(d,p) [#]	0	0.01	0.77	1.39	2.22
M06-2X/aug-cc-pVDZ[#]	0	0.03	1.09	1.57	2.66
MP2/6-311++g(d,p)	0.04	0	0.37	1.34	1.85
MP2/aug-cc-pVDZ	0	0.08	0.68	1.33	2.10

[#] *All M06-2X/ calculations were performed using the opt=tight int=ultrafine command in G09*

Table 4.3: Relative populations (as percentage) of different conformers at room temperature.

Level of Theory	Conformers				
	$G^{\pm}G^{\pm}$	$G^{\pm}G^{\mp}$	$EG^{\pm}$	$G^{\pm}E'$	EE'
B3LYP/6-311++g(d,p)	42.5	42.6	9.6	3.7	1.6
B3LYP/aug-cc-pVDZ	46.3	43.5	6.5	2.9	0.8
M06-2X/6-311++g(d,p)	46.0	44.9	6.3	2.2	0.5
M06-2X/aug-cc-pVDZ	48.3	45.9	3.8	1.7	0.3
MP2/6-311++g(d,p)	41.1	44.0	11.7	2.3	1.0
MP2/aug-cc-pVDZ	47.7	41.5	7.6	2.5	0.7
Degeneracy	2	2	1	1	1

4.2 Conformational analysis using frequency calculations and experimenta

Propofol molecule bears a hydroxy (-OH) group, which appears to be sensitive to the conformation of the molecule. Our conformational analysis of propofol is therefore based on the characterisation of vibrational frequency of the -OH bond. Frequency calculations were performed at different levels of theory and employing different basis sets using the Gaussian09 suite of programs.

Table 4.4: The computed scaled wavenumbers (cm^{-1}) of the phenolic O-H stretch conformers and the relative intensities at the MP2/-6311++g(d,p) level of theory. Scaling factors are calculated with respect to H_2O asymmetric stretch peak for the matrix used.

Matrix	**Scaling Factor**	**Conformers**				
		$G^{\pm}G^{\pm}$	**$G^{\pm}G^{\mp}$**	**$EG^{\pm}$**	**$G^{\pm}E'$**	**EE'**
N_2	0.9306	3590.8	3593.3	3588.1	3624.0	3623.0
Ar	0.9315	3594.3	3596.8	3591.7	3627.6	3626.6
Relative Intensity at 298K [##]		27.7	30.1	8.0	2.6	1.1

[##]*Computed intensities scaled with respect to relative populations at room temperature*

4.2.1 Experimental section:

A comparison between the liquid propofol and a regular matrix isolated propofol IR spectrum is given in **Fig. 4.4**, which clearly reveal the spectral resolution offered by matrix isolation, which renders it possible to delineate conformations.

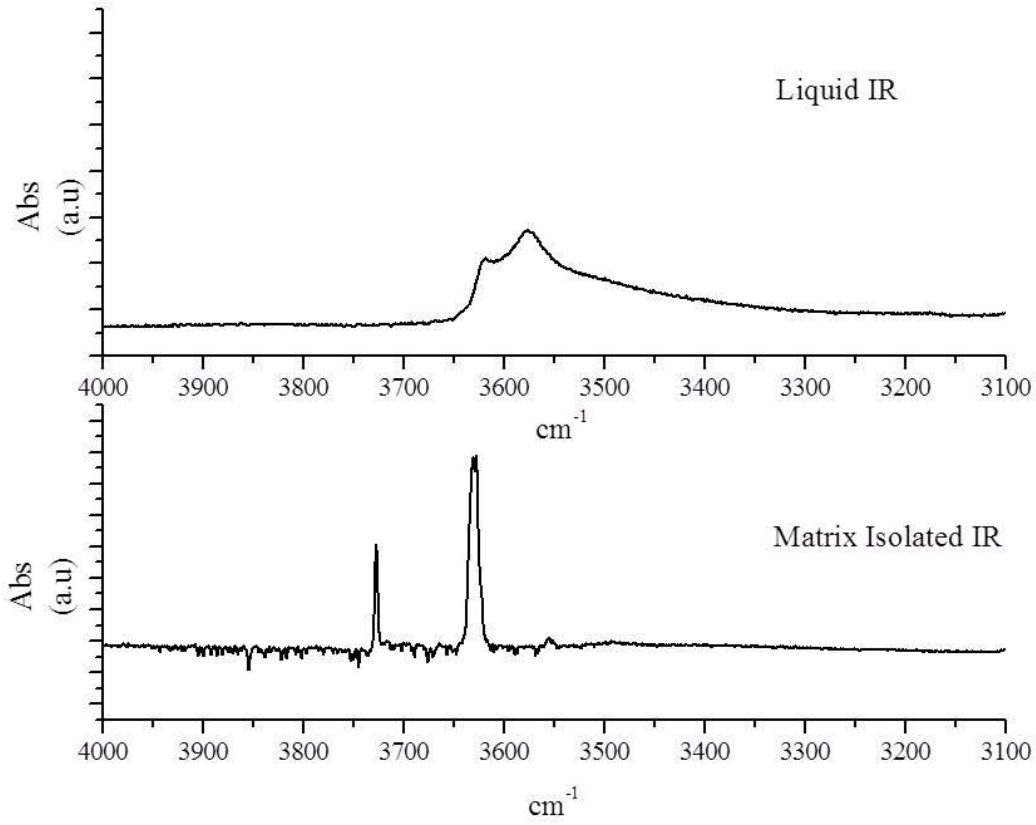

Fig. 4.4: Comparison between Liquid IR and MI-FTIR spectra of propofol

Experiments were carried out using propofol (medical grade and Sigma Aldrich 97%). The purity of the sample was confirmed using NMR and HRMS. The sample was loaded onto a double jet assembly and spectra were recorded as per specifications as mentioned in chapter 3. Spectra were recorded at 12K before and after the annealing processes. The –OH stretch mode for the conformers lie in the range of 3600-3700cm^{-1} of an IR spectrum. This forms the region of interest for the conformational analysis of the molecule, based on the identity of the characteristic –OH stretch frequency of each conformer.

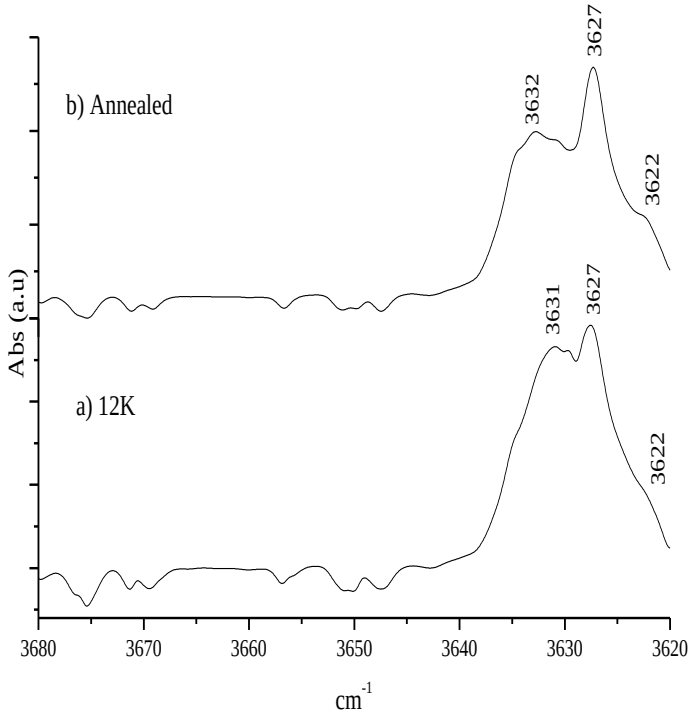

Fig. 4.5: Propofol in N_2 matrix. Propofol was maintained at 278K during deposition of the matrix. a) Spectrum recorded at 12K b) Annealed spectrum at 27-12K

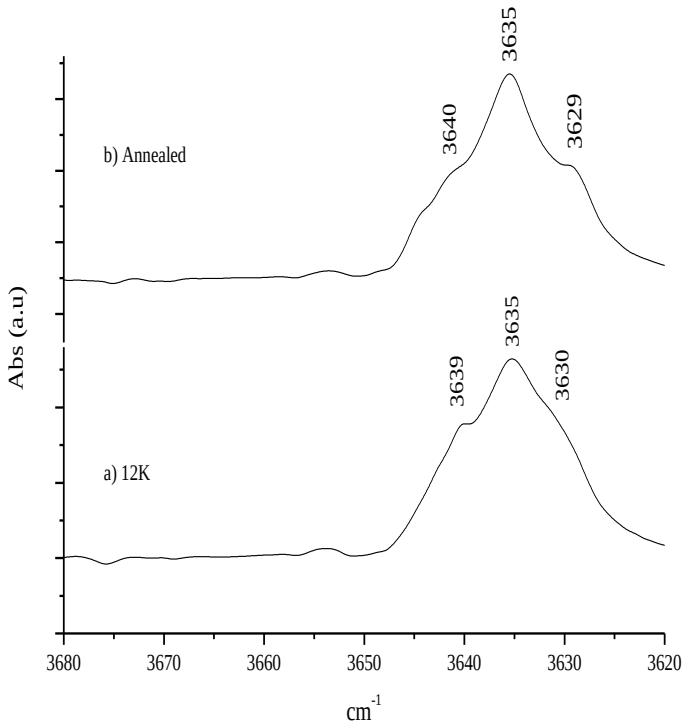

Fig. 4.6: Propofol in Ar matrix. Propofol was maintained at 288K during deposition of the matrix. a) Spectrum recorded at 12K b)Annealed spectrum at 32-12K

The spectra shown above clearly reveal that the propofol –OH feature is composed of 3 distinct peaks overlapping with each other. The two major peaks may be attributed to the $G^{\pm}G^{\mp}$ and the $G^{\pm}G^{\pm}$ conformer and are separated by ~4 cm^{-1} in each case .Another low intensity peak arising as a hump on the feature is red shifted from the major peak by $5cm^{-1}$. This peak may be assigned to the –OH stretching frequency of the $EG^{\pm}$ monomer. These assignments are made by comparing these experimental features with the computed spectra which are shown in **Fig. 4.7** and **Fig. 4.8**.

The computed spectra were obtained the MP2/6-311++g(d,p) calculations. The spectra were simulated using a Lorentzian line shape with a peak width of 1 and 3 cm^{-1}.

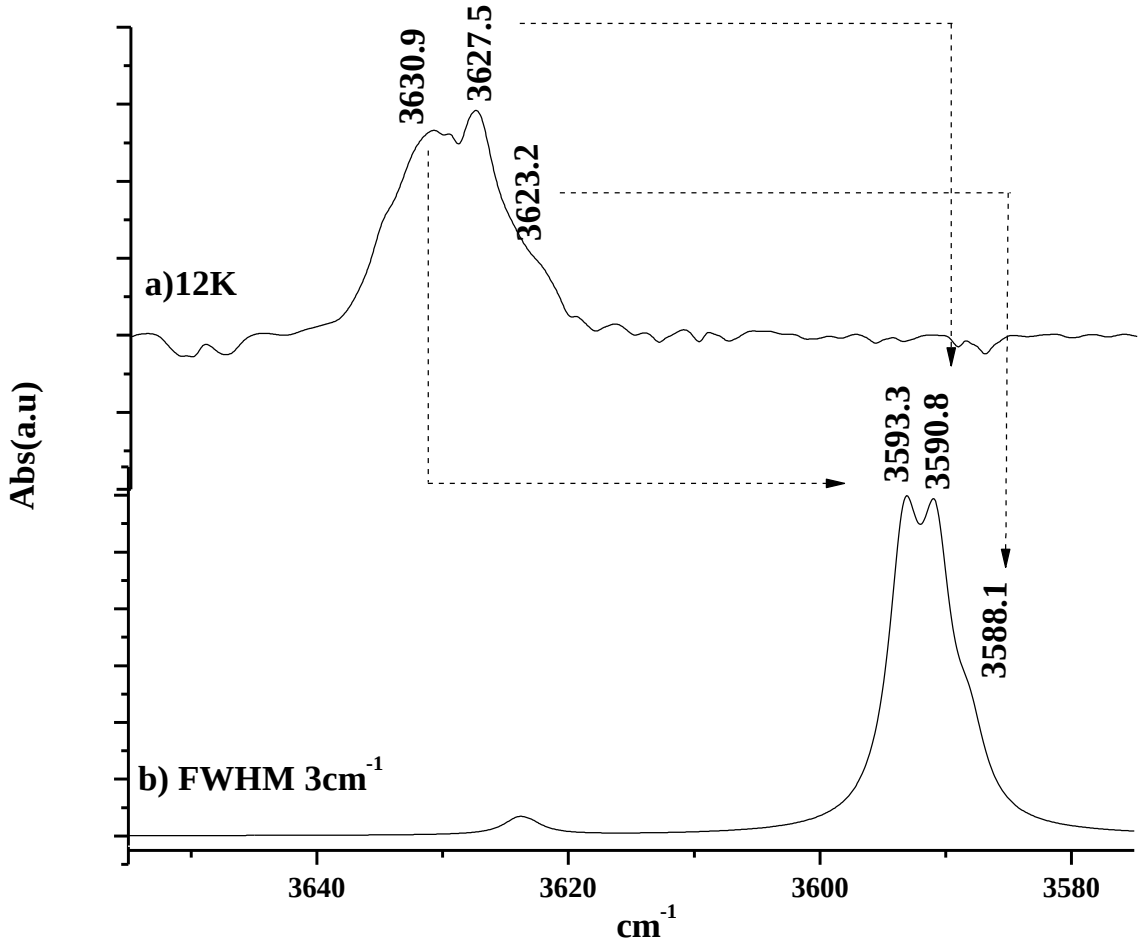

Fig. 4.7: A comparison between computed and experimental data for N_2 matrix 12K spectrum of Propofol maintained at 278K :60mb deposition and Computed (MP2/6-311++g(d,p)) spectrum simulated with a Lorentzian linewidth of $3cm^{-1}$.

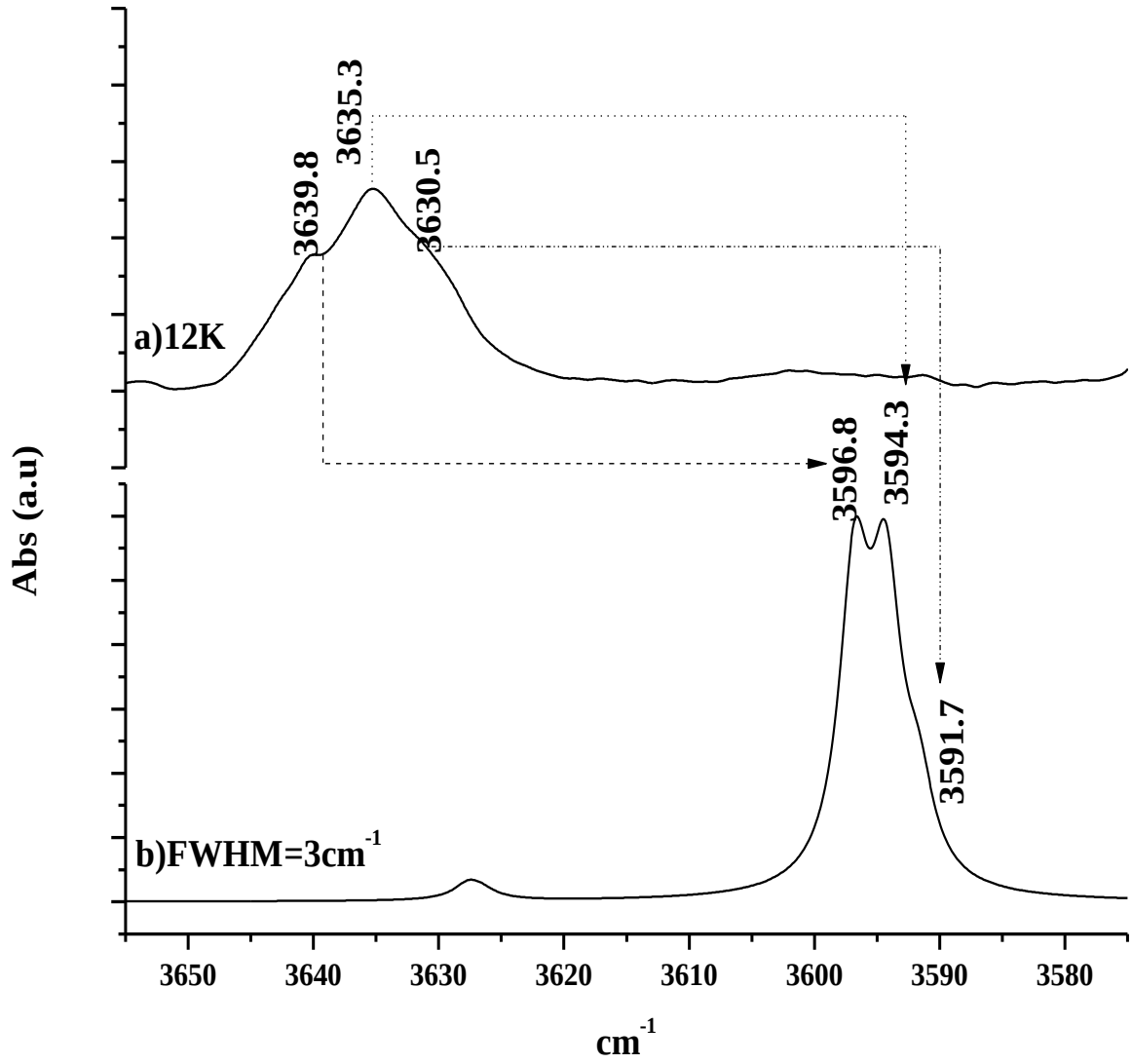

Fig. 4.8: A comparison between computed and experimental data for Ar matrix 12K spectrum of propofol maintained at 288K :60mb deposition and Computed (MP2/6-311++g(d,p)) spectrum simulated with a Lorentzian linewidth of $3cm^{-1}$.

It can be clearly seen that the experimental spectrum agrees well with the computed spectra for the conformers $G^{\pm}G^{\mp}$, $G^{\pm}G^{\pm}$ and the $EG^{\pm}$ of propofol. The EE' and $G^{\pm}E$' conformers have a very low population at room temperature and are therefore not expected to contribute to the experimental spectra recorded using the room temperature sample.

4.3 Vibrational assignments

The assignment of the features obtained in **Fig. 4.7** and **Fig. 4.8.** has been done in **Table 4.5.**

Table 4.5: A comparison of the MP2/6-311++g(d,p) computed and experimental wavenumbers for the three conformers for the –OH stretch of the propofol molecule. The computed wavenumbers were scaled.

Conformers	N_2 matrix		Ar matrix	
	Computed	Experimental	Computed	Experimental
$G^{\pm}G^{\mp}$ (GG)	3593.3	3630.9	3596.8	3639.8
$G^{\pm}G^{\pm}$ (Gg)	3590.8	3627.5	3594.3	3535.3
$G^{\pm}G^{\pm}$ (EG)	3588.1	3623.2	3591.7	3630.5

From the assignments given in **Table4.4,** it can be seen that $G^{\pm}G^{\mp}$, $G^{\pm}G^{\pm}$ and $EG^{\pm}$ conformers are identified in the matrix.

4.4 Discussion

We now discuss the consequences of molecular conformations on the chemical activity of the molecule. Lessari et. al and Fernandez et. al [8,11,14,15,56] have reported the presence of $EG^{\pm}$, $G^{\pm}E$' and the $G^{\pm}G^{\pm}$ conformers in their studies. Both comment on the low barrier of interconversion of the $G^{\pm}G^{\mp}$ and $G^{\pm}G^{\pm}$, and cite it as a reason for not being to identify separately the two conformers, in their CP-FTMW, UV/UV hole burning, IR-IDS and 2 colour REMPI experiments. However, matrix isolation experiments, due to the operation of the cage effect preserves the various conformers present in the room temperature gas phase sample, and allows for their detection. Conformer interconversion is essentially discouraged in the matrix which allows for their individual identification. Our *ab-intio* computations corroborate the presence of the $G^{\pm}G^{\mp}$, $G^{\pm}G^{\pm}$ and the $EG^{\pm}$ conformers in the matrix. The $G^{\pm}E$' and EE' conformers could not be observed in the experimental spectrum due to their low populations.

In order to see if the conformational population could be altered by varying the temperature of the sample prior to deposition, we tried using supersonic expansion coupled with MI-FTIR. This combination of supersonic jet-matrix isolation was demonstrated to be a powerful method by Viswanathan et al[57] to alter conformational population which leads to

unambiguous assignments of the conformers in the matrix. Supersonic jet expansion experiments were carried out using Parker Iota One Pulse Driver controlled pulsed valve unit with a backing pressures of 1 bar of matrix gas. However the very low vapour pressure of propofol prevented enough sample to be deposited onto the matrix and hence vibrational features of propofol could not be obtained. Alternate design and instrumental modification may have to be devised to perform supersonic jet-matrix isolation experiments with propofol. To summarize, matrix isolation studies clearly indicate the presence of the $G^{\pm}G^{\mp}$, $G^{\pm}G^{\pm}$ and the $EG^{\pm}$ conformer to be present, trapped in the matrix.

Chapter 5

Interaction studies of propofol and H_2O

5.1 Introduction

The anaesthetic properties of propofol have been linked to the reactivity of the phenolic group in the molecule. Several studies discuss the chemical reactivity of propofol with other molecules that are responsible for its anaesthetic properties. X-ray crystal structure studies by Evers and Franks and Nury et. al discuss in detail[12], biological binding sites of propofol on the receptors of the neurotransmitter $GABA_A$. As described by Evers and Franks,[12] the propofol molecule docks onto the tryptophan and the threonine residues of the $GABA_A$ receptor. Both amino acids are known to interact with the molecule through the hydroxyl groups. Thus, the chemistry of the molecule and its biological action rests upon the hydrogen bonding activity of the phenolic –OH group. Fernandez, Castano and Lessari8,[11,13-15] have extensively looked into propofol's chemical interactions of propofol with molecules such as isopropanol, phenol and H_2O, employing a variety of spectroscopic techniques.

Fernandez et.al [11,13-15] have studied propfol-H_2O complexes in jets using techniques such as REMPI, UV/UV double resonance and IRIDS. These results have probed the propofol- H_2O clusters in the gas phase, where only the global minimum is sampled. Matrix isolation studies have known to yield results different from gas phase studies due to the operation of the cage effect and very often have even been found to observe local minima, which go unobserved in gas phase studies.[58,59] Thus, it is worthwhile to analyse the propofol- H_2O complex using matrix isolation experiments.

In chapter 4, we presented our studies of the conformers of propofol and established that the $G^{\pm}G^{\mp}$, $G^{\pm}G^{\pm}$ and $EG^{\pm}$ conformers are identified in the matrix. Given the multiplicity of conformations, the hydrogen bonding landscape becomes rich and complicated, with numerous possibilities of hydrogen bonded isomers. Furthermore, the different hydrogen bonding sites in propofol and H_2O adds to the complexity. Our aim is to identify the stable interactions of the molecule using matrix isolated FTIR spectroscopy and *ab initio* calculations.

5.2 Possible sites of interaction

The phenol-H_2O system has been studied using matrix isolation FTIR spectrposcopy and *ab initio* studies by Gor et. al.[9] Using computations, they reported three possible binding sites for the H_2O molecule on phenol. First was the phenol molecule as a proton donor to the oxygen atom on H_2O, the second was H_2O acting as a proton donor to the phenolic oxygen and the third was hydrogen atoms of H_2O interacting with the π electron cloud of phenol. Experimentally they observed the complex where phenol served as the proton donor to H_2O. This is consistent with the fact that the phenolic hydrogen is more acidic than that of H_2O, as indicated by their pKa values. The experimentally observed infrared spectrum shows a red shift of ~ -180 cm^{-1} for the stretch of phenolic group.

The propofol molecule, being a phenol analogue can be expected to show similar chemistry. Propofol however is different from phenol as the bulky isopropyl groups ortho to the phenol group, renders the interaction of propofol with H_2O dependent on the conformation of propofol. One therefore expects a characteristic shift in the stretching frequency of the normal modes for the complexes involving the different conformers of propofol. It is this difference rendered by the isopropyl group that makes the molecule selective to several biological processes which involve binding through interactions like hydrogen bonding. Thus study of these complexes gives a significant insight into the possible biological activity of the molecule.

5.3 Computational details

The possible 1:1 complexes of propofol and H_2O have been abbreviated as the following:

a) **Ppf-W** : Propofol acts as a proton donor to the H_2O molecule
b) **W-Ppf** : H_2O as a proton donor to the propofol molecule
c) **H-π** : The interaction of H_2O with the π electron cloud of the propofol molecule.

Superimposed on the three different possibilities mentioned above, each conformer of propofol can interact with H_2O to yield a large number of isomers for the hydrogen bonded complex, which are shown in **Fig. 5.1.a-n**.

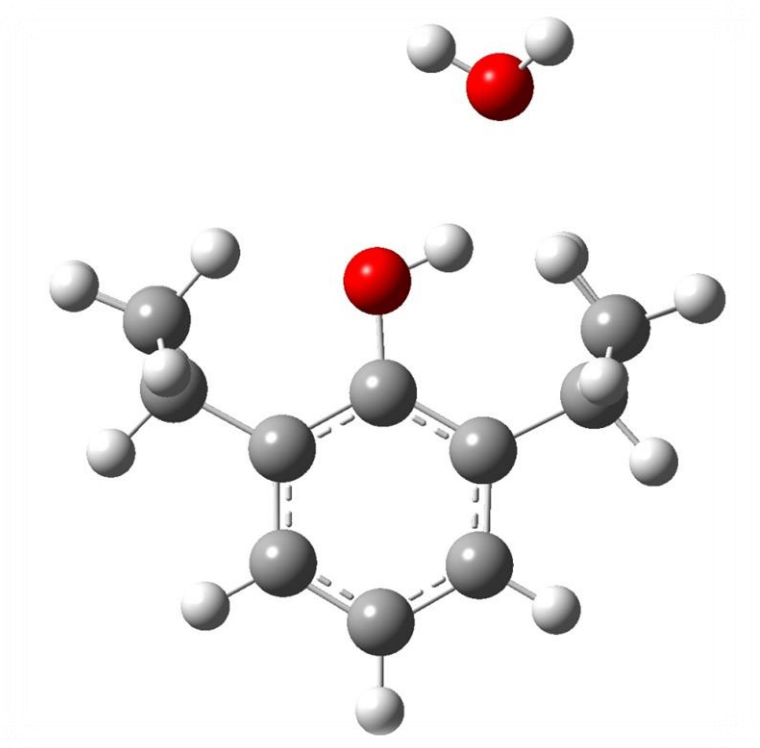

Fig. 5.1.a: EE’ Ppf-W

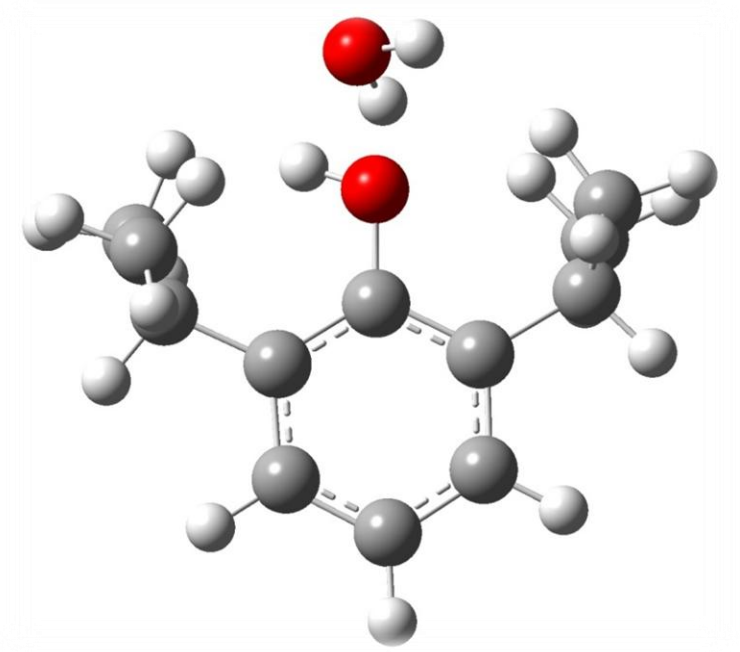

Fig. 5.1.b: EE’ W-Ppf

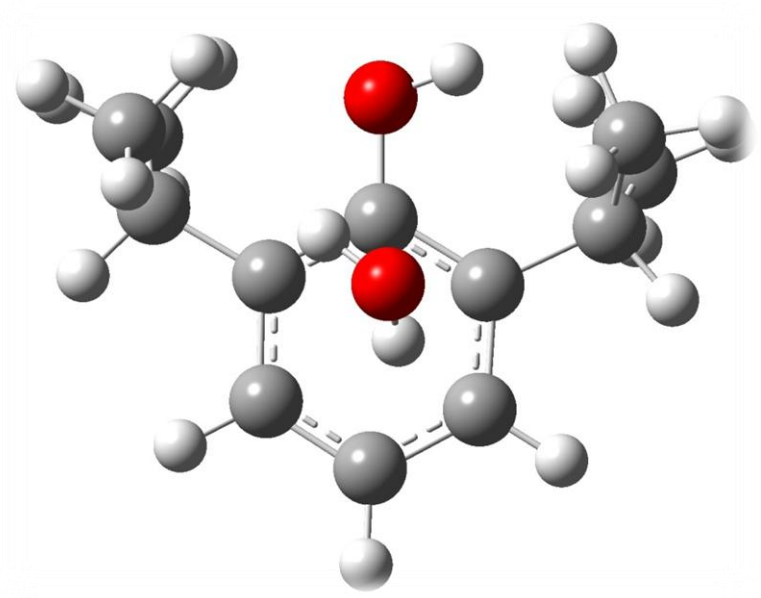

Fig. 5.1.c: EE’ H-π

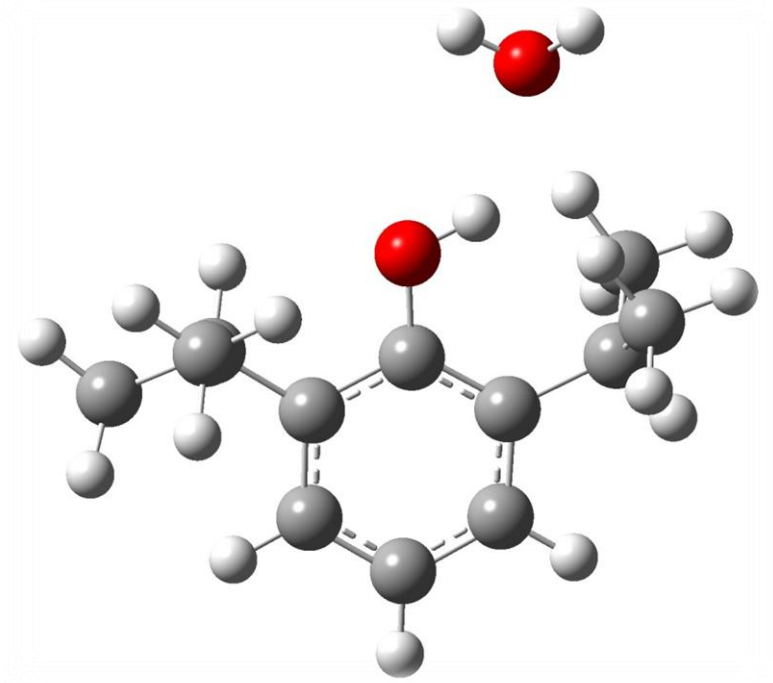

Fig. 5.1.d: $G^{\pm}E$’ PPf-W

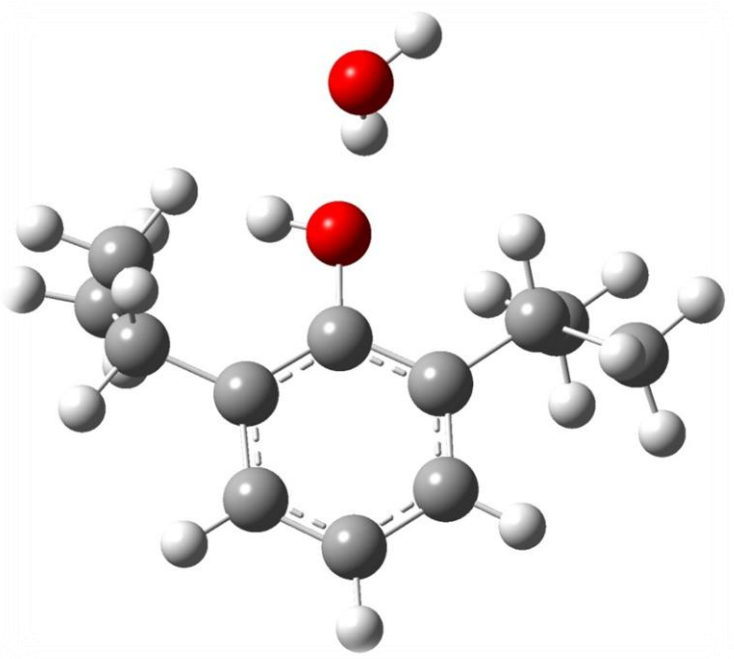

Fig. 5.1.e: $G^{\pm}E'$ W-Ppf

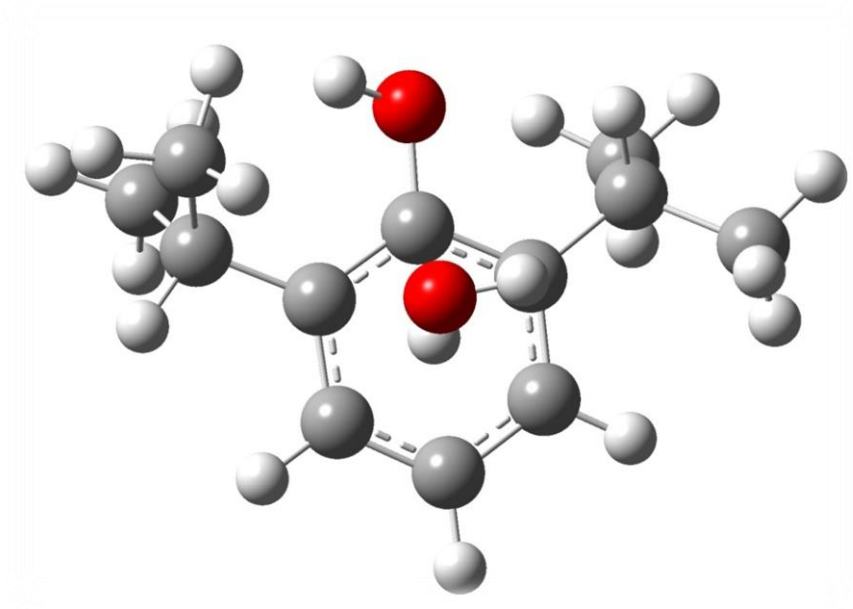

Fig. 5.1.f: $G^{\pm}E'$ H-π

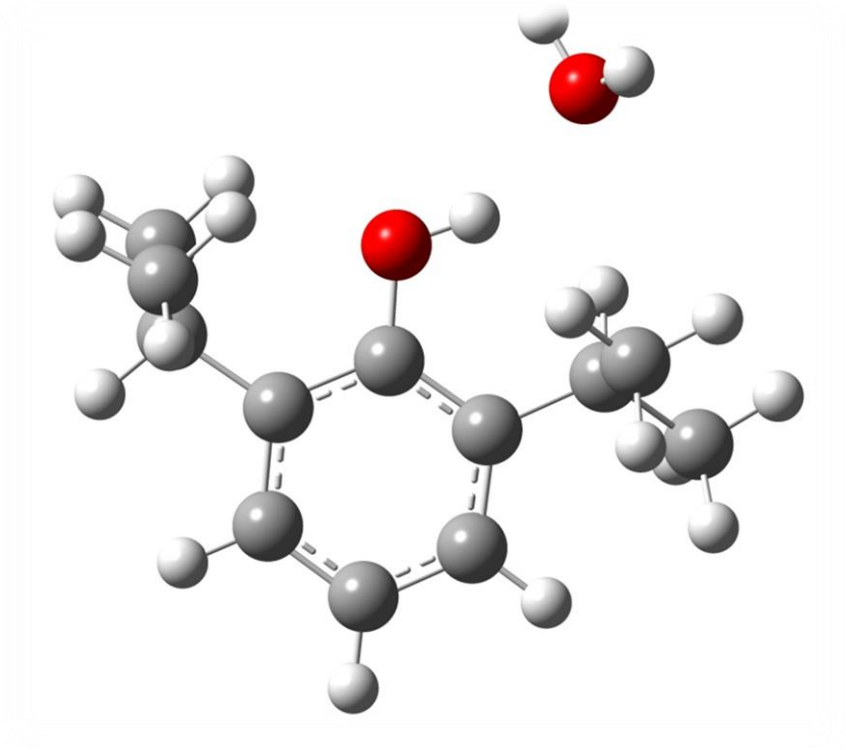

Fig. 5.1.g: $EG^{\pm}$ PPf-W

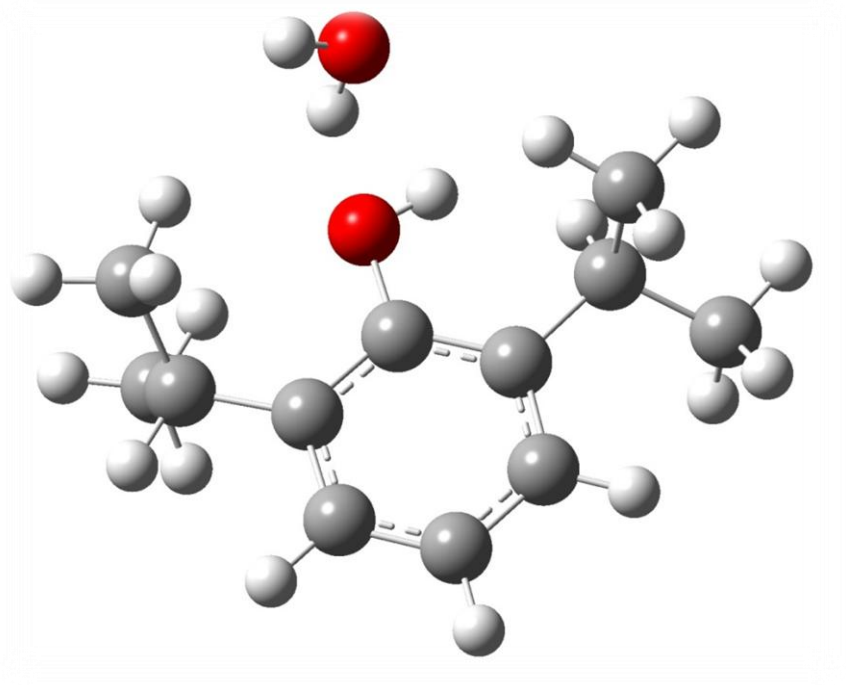

Fig. 5.1.h: $EG^{\pm}$ W-Ppf

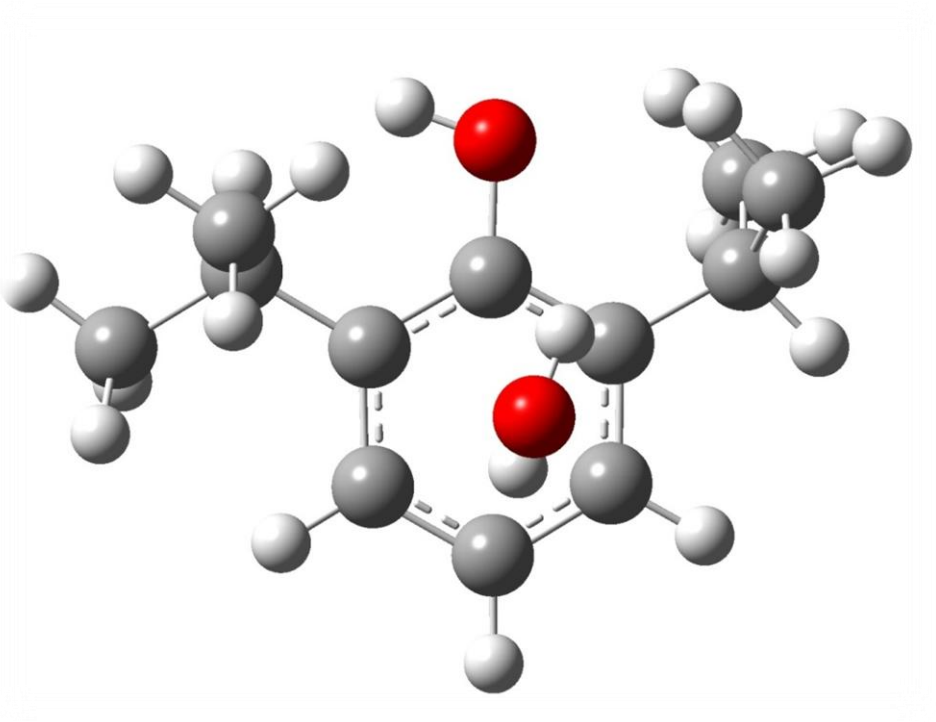

Fig. 5.1.i: $EG^{\pm}$ H-π

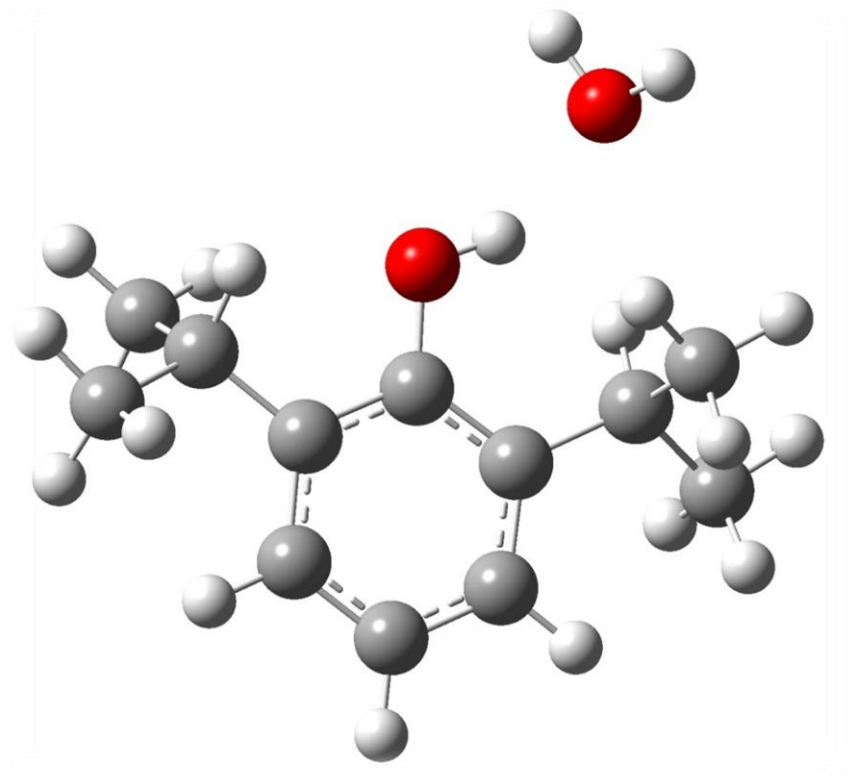

Fig. 5.1.j: $G^{\pm}G^{\mp}$ Ppf-W

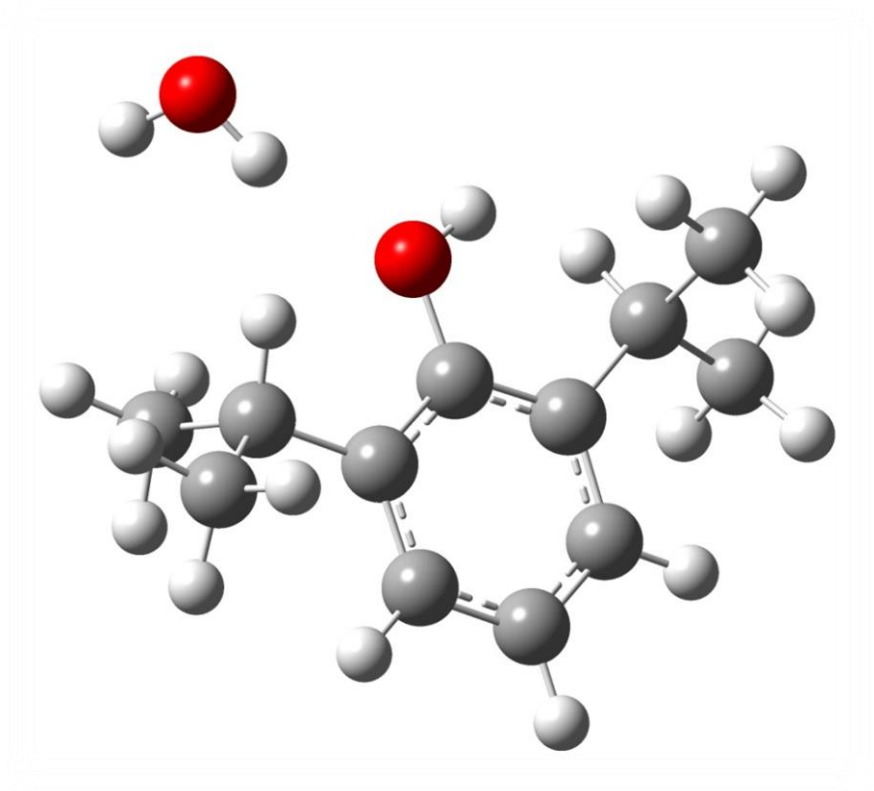

Fig. 5.1.k: $G^{\pm}G^{\mp}$ W-Ppf

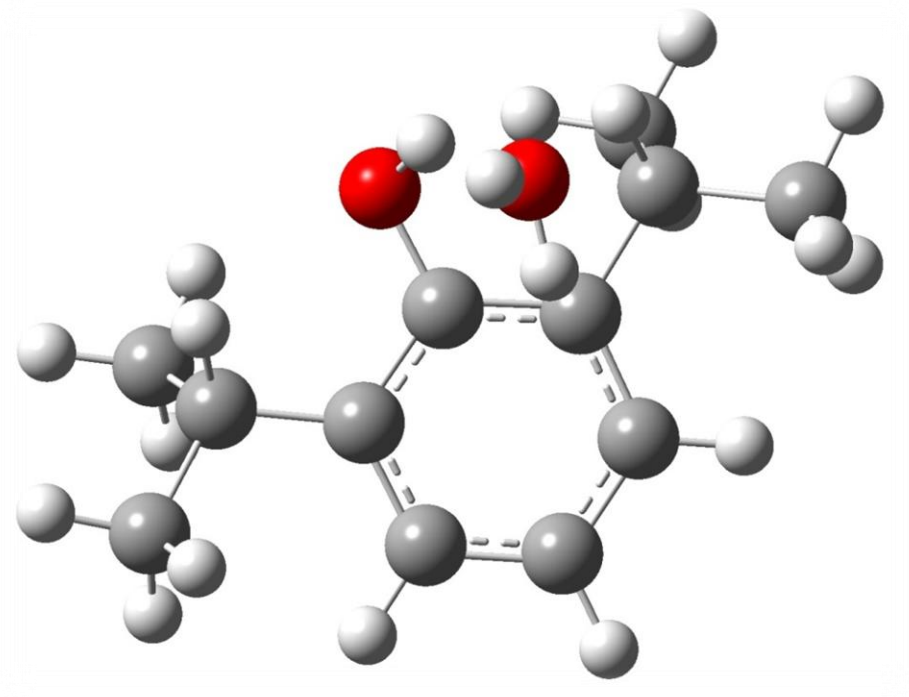

Fig. 5.1.l: $G^{\pm}G^{\mp}$ H-π + Ppf-W

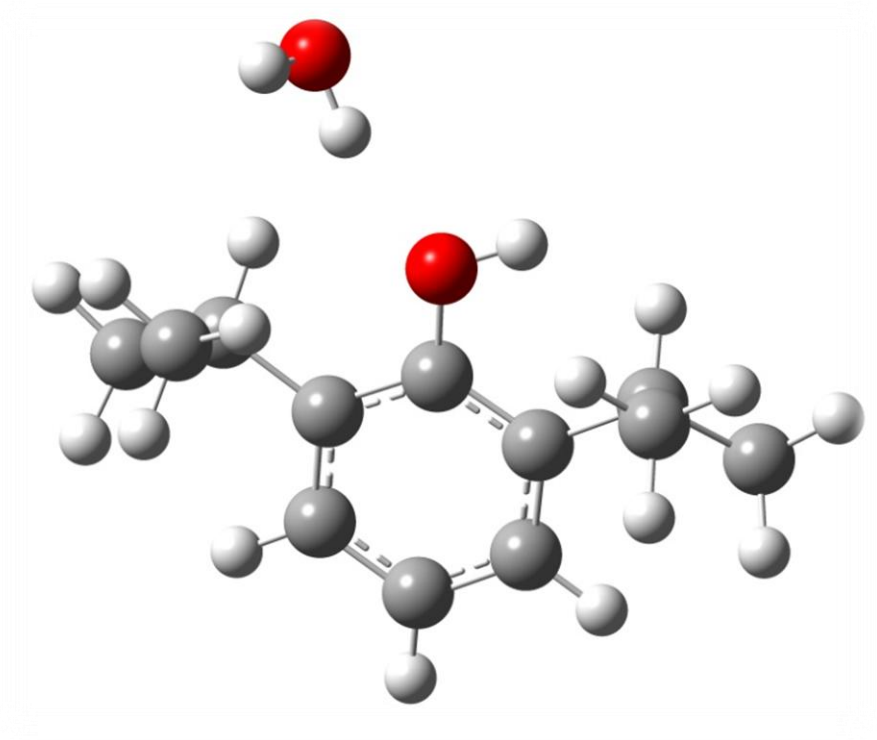

Fig. 5.1.m: $G^{\pm}G^{\pm}$ W-Ppf

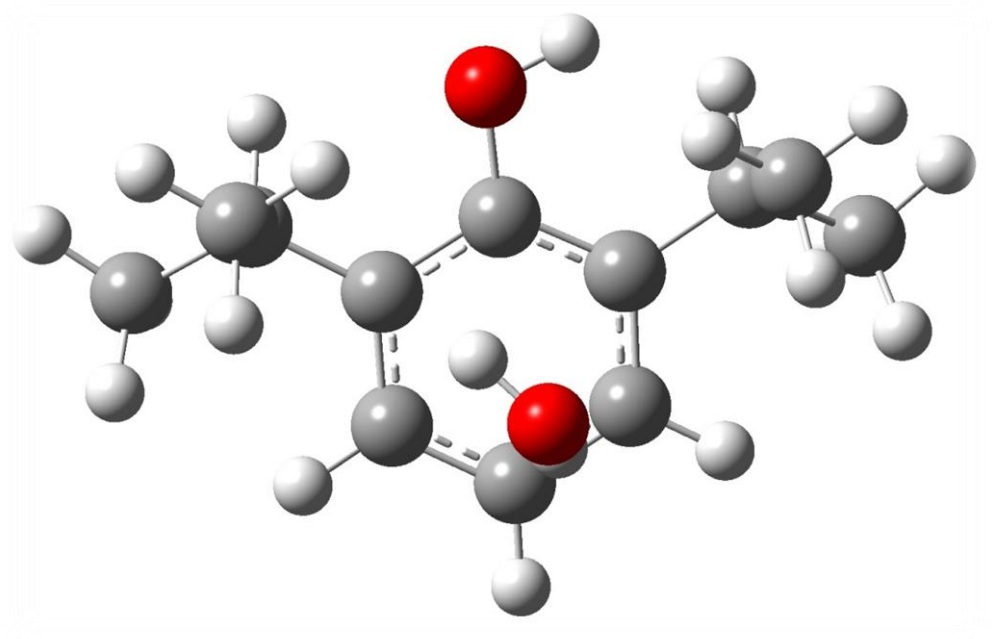

Fig. 5.1.n: $G^{\pm}G^{\pm}$ H-π

Computations indicate a conformational switching of the $G^{\pm}G^{\pm}$-Ppf-W complex to the $G^{\pm}G^{\mp}$-Ppf-W complex, which is energetically the global minimum structure. When H_2O forms a complex with propofol, the $G^{\pm}G^{\pm}$ conformer switches to a $G^{\pm}G^{\mp}$ conformer and forms a complex with the structure $G^{\pm}G^{\mp}$-Ppf-W. Another interesting complex was indicated in the case of the $G^{\pm}G^{\mp}$-H- π system at the MP2 and the M06-2X levels of theory. In this case the H_2O molecule orients itself in a fashion such that the phenolic –OH group is pushed out of the aromatic plane. This results in a dual interaction, with the phenolic proton interacting with the oxygen of H_2O in an out of the plane fashion, as well as the H- π interaction. **Table 5.1** gives the consolidated list of all the complexes with their energies, so that the energy ordering can be recognized for the various complexes, all of which have been checked to be minima on the potential surface using vibrational frequency calculations.

Table 5.1: Stabilization energies of the complexes with respect to the monomers (uncorrected/ ZPE corrected/BSSE corrected). All values in kcal/mol.

	B3LYP		**M06-2X**		**MP2**	
Complex	***6-311++g(d,p)***	***aug-cc-pVDZ***	***6-311++g(d,p)***	***aug-cc-pVDZ***	***6-311++g(d,p)***	***aug-cc-pVDZ***
PPf(EE')-W	-4.46/-3.22 /-3.52	-3.66/-2.52 /-3.02	-7.16/-5.71 /-6.09	-6.12/-4.75 /-5.40	-6.80/-5.36 /-4.11	-6.40
W-PPf(EE')	-3.68/-2.27 /-3.02	-3.66/-2.52 /-2.98	-6.07/-4.38 /-5.11	-5.67/-3.98 /-4.89	-6.11/ 4.04 /-3.53	-6.11
H-π PPf(EE')	-3.16/-2.22 /-2.41	-2.78/-1.13 /-2.17	-7.28/-5.90 /-6.09	-6.48/-4.22 /-5.69	-4.11/-3.53 /-3.80	*-6.56**
PPf($G^{\pm}E'$)-W	-4.50/3.22 /-3.96	-3.69/-1.97 /-3.11	-7.22/-5.67 /-6.16	-6.16/-4.83 /-5.47	-6.78/-5.33 /-4.12	-6.39
W-PPf($G^{\pm}E'$)	-4.05/-2.58 /-3.33	-3.69/-2.50 /-3.11	-6.97/-5.43 /-5.73	-5.11/-3.77 /-4.40	-6.19/-4.24 /-3.79	-6.09
H-π PPf($G^{\pm}E'$)	-3.21/-2.18 /-2.44	-2.81/-1.73 /-2.21	-6.91/-5.72 /-5.69	-6.07/-4.95 /-5.17	-6.90/-5.54 /-3.92	*-6.95**
PPf($EG^{\pm}$)-W	-5.46/-3.92 /-4.41	-4.53/-3.15 /-3.74	-8.22/-6.38 /-7.05	-7.24/-5.61 /-6.45	-7.57/-5.94 /-4.85	-7.45
W-PPf($EG^{\pm}$)	-3.85/-2.22 /-3.06	-3.38/-1.90 /-2.54	-6.17/-4.27 /-5.16	-5.51/-3.98 /-4.76	-6.13/-4.24 /-3.65	-6.16
H-π PPf($EG^{\pm}$)	-2.94/-1.85 /-2.25	-2.57/-1.54 /-1.96	-7.15/-5.85 /-5.94	-6.40/-5.12 /-5.57	-6.58/-5.38 /-3.51	*-6.59**

PPf($G^{\pm}G^{\mp}$)-W	**-5.48/-3.77 /-4.43**	**-4.58/-3.18 /-4.01**	**-8.24/-6.41 /-7.07**	**-7.23/-5.55 /-6.48**	**-7.58/-5.91 /-4.86**	**-7.44**
W-PPf($G^{\pm}G^{\mp}$)	-4.17/-2.58 /-3.54	-3.44/-2.08 /-2.96	-6.28/-4.54 /-5.41	-5.55/-4.11 /-4.91	-5.72/-4.04 /-3.59	-5.90
H-π PPf($G^{\pm}G^{\mp}$)	- 3.09/-2.18/-1.90	-2.77/-1.64/-2.18	*Optimizes to* ***{Ppf-W+ H-π* PPf} ($G^{\pm}G^{\mp}$)**			
{Ppf-W+ H-π PPf} ($G^{\pm}G^{\mp}$)	Optimizes to ***$G^{\pm}G^{\mp}$-Ppf-W***		-7.50/-5.97 /-6.46	-6.34/4.95 /-5.49	-7.26/-5.64 /-4.40	*-6.89**
PPf-W ($G^{\pm}G^{\pm}$)	**Optimizes to *$G^{\pm}G^{\mp}$-Ppf-W***					
W-PPf($G^{\pm}G^{\pm}$)	-4.07/-2.46 /-3.34	-3.44/-2.08 /-2.96	-6.29/-4.55 /-5.41	-5.53/-4.05 /-4.91	-5.92/-4.25 /-3.72	-5.89
H-π($G^{\pm}G^{\pm}$)	-2.88/-1.91 /-2.05	-2.57/-1.53 /-2.04	-7.33/-6.14 /-6.14	-6.61/-5.35 /-5.77	-6.82/-5.69 /-3.66	*-6.95**

*Indicates single point energies calculated on the MP2/6-311++g(d,p) geometry #M06-2x calculations done using opt=tight, int=ultrafine command on G09.

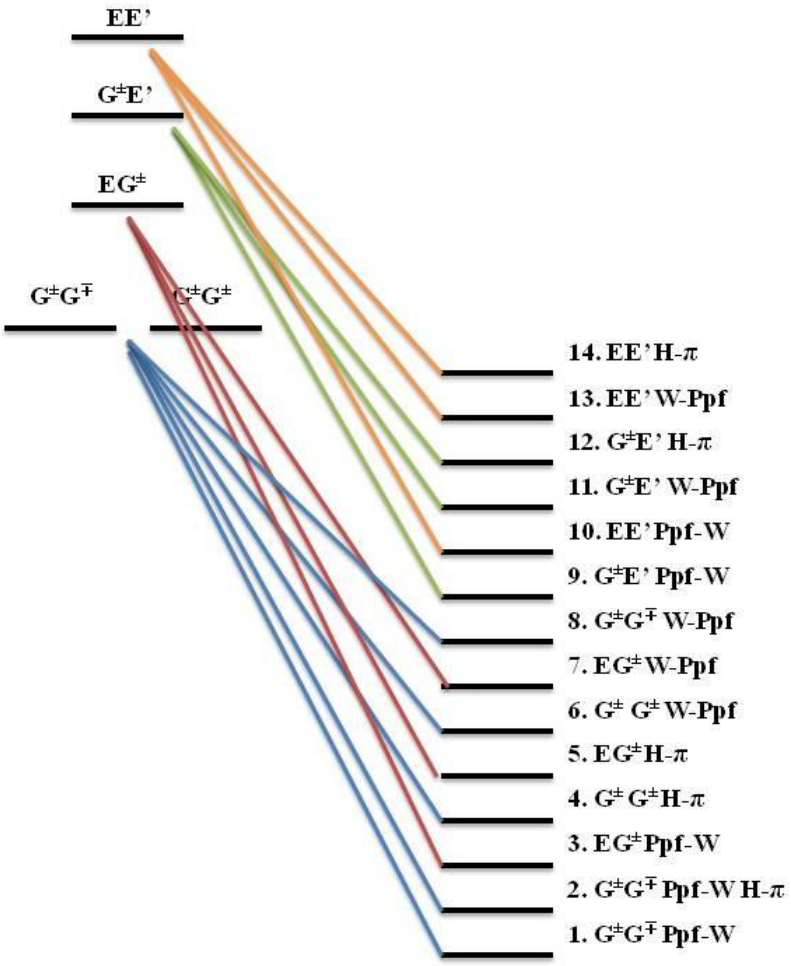

Fig. 5.2: The relative ordering of the complexes with respect to their energies computed at the MP2/6-311++g(d,p)). The diagram shows the correlation of the complexes with the respective monomers, which also has been ordered with respect to their energies. Energies are not to scale.

Hence it is clear that the $G^{\pm}G^{\mp}$-Ppf-W is energetically the most stable complex among all the possible isomeric complexes. The frequency calculations were used to assign the vibrational features in the matrix isolation experiments. The complexation of H_2O with propofol leads to a perturbation in the characteristic frequencies of vibration of the monomers. In order to confirm the formation of the complex, these shifts are compared to the shifts obtained from the assigned observed features in the experimental spectra. In accordance to the relative stability of the complexes and the observed shifts in the experiments it is possible to identify the complexes trapped in the matrix. **Table 5.2** indicates the scaled computed frequencies and the shifts observed on complexation.

Table 5.2: Scaled computed wavenumbers (cm^{-1}) and the calculated shifts (in parenthesis) for the various complexes optimized at the MP2/6-311++g(d,p) level, relevant for the N_2 matrix.

H_2O Asym –OH	3727.5		
	Ppf-W	**W-Ppf**	**H-π**
EE'	3628.5		
Ppf-OH stretch	3572.0 (**-56.5**)	3593.6 (**-34.9**)	3610.4 (**-18.1**)
W-OH asym stretch	3708.2 (**-19.3**)	3692.9 (**-34.6**)	3683.7 (**-43.8**)
$G^{\pm}E'$	3629.5		
Ppf-OH stretch	3569.6 (**-59.9**)	3605.8 (**-23.7**)	3611.4 (**-18.1**)
W-OH asym stretch	3708.8 (**-18.7**)	3691.6 (**-35.9**)	3692.2 (**-35.3**)
$EG^{\pm}$	3593.7		
Ppf-OH stretch	3504.0 (**-89.7**)	3569.1 (**-24.6**)	3588.8 (**-4.9**)
W-OH asym stretch	3705.8 (**-21.7**)	3692.7 (**-34.8**)	3684.9 (**-42.6**)
$G^{\pm}G^{\mp}$	3598.8		
Ppf-OH stretch	3503.6 (**-95.2**)	3588.9 (**-9.9**)	3510.3 (**-88.5**)[#]
W-OH asym stretch	3706.1 (**-21.4**)	3696.8 (**-30.7**)	3693.6 (**-33.9**)
$G^{\pm}G^{\pm}$	3596.2		
Ppf-OH stretch	Optimizes to $G^{\pm}G^{\mp}$PpfW	3582.6 (**-13.6**)	3593.7 (**-2.5**)
W-OH asym stretch		3696.5 (**-31.0**)	3685.7 (**-41.8**)

Scaling factors as shown in Table 4.4

Table 5.3: Scaled computed wavenumbers (cm^{-1}) and the calculated shifts (in parenthesis) for the various complexes optimized at the MP2/6-311++g(d,p) level, relevant for the Ar matrix.

H_2O Asym –OH	3731.0		
	Ppf-W	**W-Ppf**	**H-π**
EE'	3631.9		
Ppf-OH stretch	3575.4/**(-56.5)**	3597.0/**(-34.9)**	3613.8/**(-18.1)**
W-OH asym stretch	3711.7/**(-19.3)**	3696.4/**(-34.6)**	3687.2/**(-43.8)**
$G^{\pm}E'$	3632.9		
Ppf-OH stretch	3573.0/**(-59.9)**	3609.2/**(-23.7)**	3614.8/**(-18.1)**
W-OH asym stretch	3712.3/**(-18.7)**	3695.1/**(-35.9)**	3695.7/**(-35.3)**
$EG^{\pm}$	3597.1		
Ppf-OH stretch	3507.3/**(-89.8)**	3572.5/**(-24.6)**	3592.2/**(-4.9)**
W-OH asym stretch	3709.3/**(-21.7)**	3696.2/**(-34.8)**	3688.4/**(-42.6)**
$G^{\pm}G^{\mp}$	3602.2		
Ppf-OH stretch	3506.9/**(-95.3)**	3592.3/**(-9.9)**	3513.6/**(-88.6$^{\#}$)**
W-OH asym stretch	3709.6/**(-21.4)**	3700.3/**(-30.7)**	3697.1/**(-33.9)**
$G^{\pm}G^{\pm}$	3599.6		
Ppf-OH stretch	Optimizes to $G^{\pm}G^{\mp}$PpfW	3586.0/**(-13.6)**	3597.1/**(-2.5)**
W-OH asym stretch		3700.0/**(-31.0)**	3689.2/**(-41.8)**

Scaling factor as shown in Table 4.4.

5.4 Experimental section

The 1:1 Ppf-W complex was prepared in the inert matrix using the technique of matrix isolation FTIR spectroscopy. The matrix gas and H_2O vapors were equilibrated in the stainless steel sample chamber while propofol was deposited using the second jet of a double jet assembly. Experiments for concentration dependence and isotopic analysis were also performed for confirming the complex features observed on the experimental spectra. The matrix gases used were N_2 and Ar and the recorded spectra for the experiments have been shown in **Fig. 5.3** and **Fig. 5.4.**

The experiments were carried out using a deposition rate of ~3mmol/hr. Since the propofol was deposited using a double jet assembly it was not possible to determine the exact concentration of propofol in the matrix. Hence using the vapour pressure data as a function of temperature, we only give relative concentrations of propofol in the various experiments.

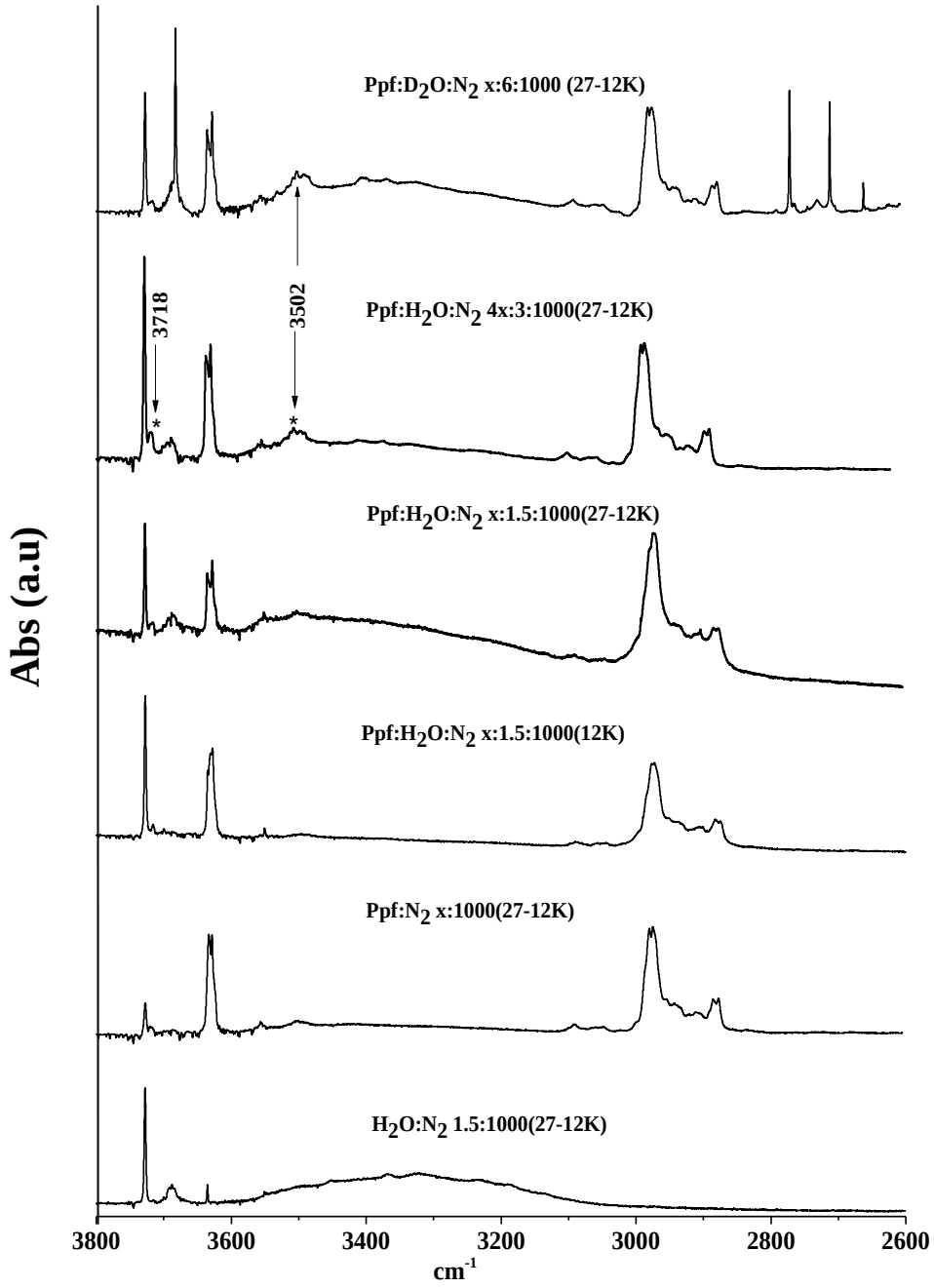

Fig. 5.3: Experimental spectrum of 1:1 Ppf: H_2O complexes in N_2 matrix. The figure shows the concentration dependence and the isotopic analysis of the complex features obtained for the Ppf: H_2O system. 'x' denotes the relative concentration of Ppf at 278K and '4x' at 288K. The two complex features obtained from these experiments are located at 3502cm^{-1} and 3718cm^{-1}. The assignments for these peaks have been discussed in the next section.

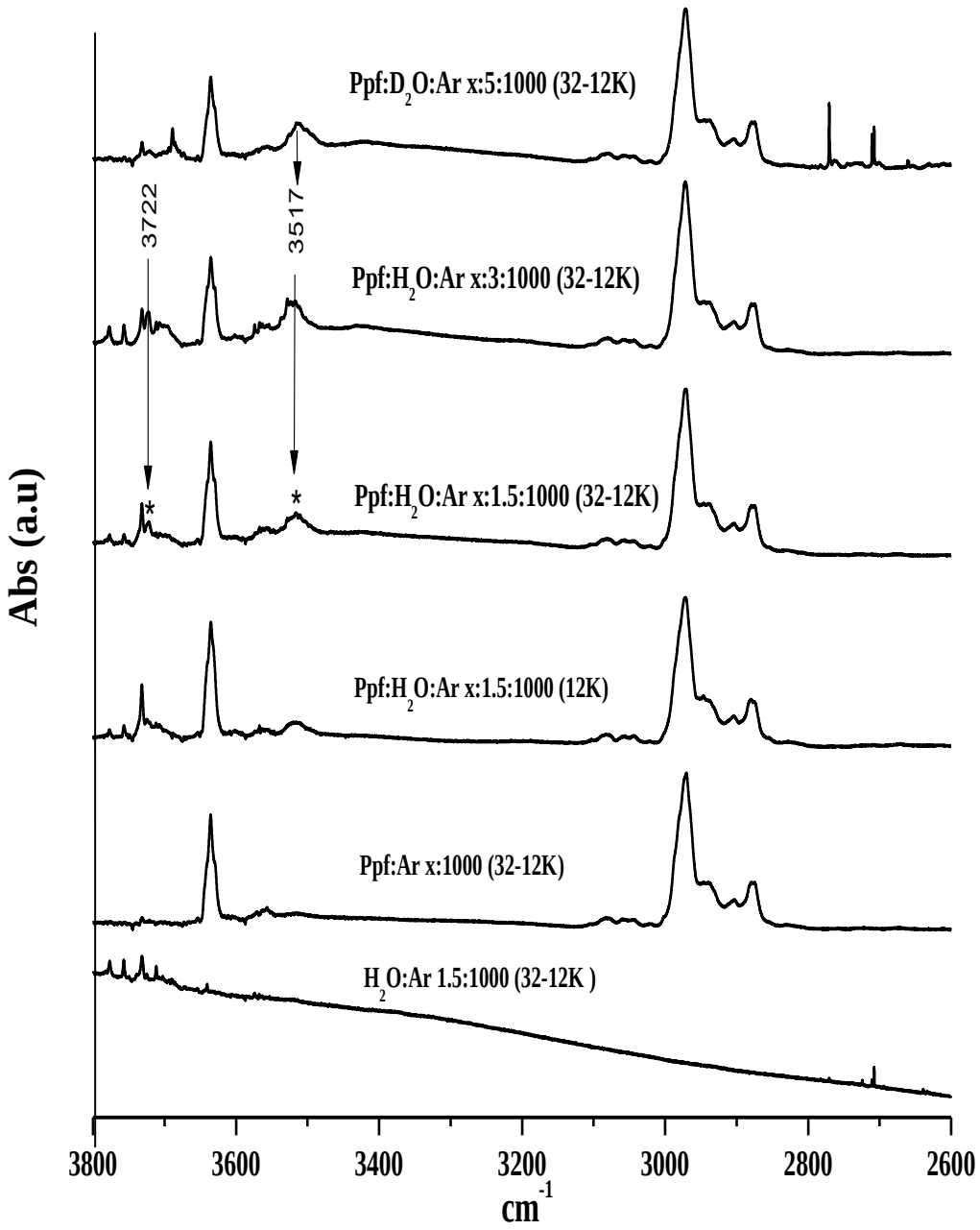

Fig. 5.4: Experimental spectrum of 1:1 Ppf: H_2O complexes in Ar matrix. The figure shows the concentration dependence and the isotopic analysis of the complex features obtained for the Ppf: H_2O system. 'x' denotes the relative concentration of Ppf at 288K. The two complex features obtained from these experiments are located at 3517cm^{-1} and 3722cm^{-1}. The assignments for these peaks have been discussed in the next section.

5.5 Discussion of the experimental spectra

In both N_2 and Ar matrices, we observe new product features following codeposition of the propofol and H_2O. Since the O-H stretching region of both propofol and H_2O is the one sensitive to complex formation, we have restricted the analysis of our data to the region of the O-H stretch which is 3800cm^{-1} -2600cm^{-1} .

As seen from **Table 5.1**, the $G^{\pm}G^{\mp}$ Ppf-W complex is the lowest in energy. This complex was found to yield a scaled computed frequency of 3503cm^{-1} for the perturbed –OH stretch of propofol in N_2. The experiments in N_2 yield a complex feature at 3502cm^{-1}. The H_2O asymmetric –OH stretch as per computations for the same is located at 3706cm^{-1}, and experimentally the complex feature at 3718cm^{-1} may be assigned to the H_2O –OH asymmetric stretch in the complex.

In the case of the experiments in Ar matrix, the computed frequency for the –OH stretch of propofol was indicated to be at 3507cm^{-1} and experimentally this was assigned to the feature at 3517cm^{-1} on the experimental spectrum obtained in an Ar matrix. Similarly, the computed frequency for the asymmetric stretch of the H_2O for Ar was at 3710cm^{-1} and experimentally this feature was found at 3722cm^{-1}.

Experiments were also done with propofol and D_2O. However, the features of the phenolic stretch of propofol appear at the same position as with H_2O, as shown in Fig 5.3 and 5.4. We have not discussed the shift in the O-D features, for which more experiments need to be done.

5.6 Atoms-in-molecules (AIM) analysis

AIM analysis of the complexes were performed on the optimized geometries of the complexes at the MP2/6-311++g(d,p) level of theory. The topological criteria for the existence of hydrogen bonding says that an electron density at the H−X(BCP) should be in the range 0.002−0.034 a.u whereas the $\nabla^2\rho(r_c)$ within 0.024−0.139.[60]

The $G^{\pm}G^{\mp}$ Ppf-W complex was analysed using the AIM2000 suite of program and the **Fig. 5.5** shows the bond paths and the critical points obtained for the complex.

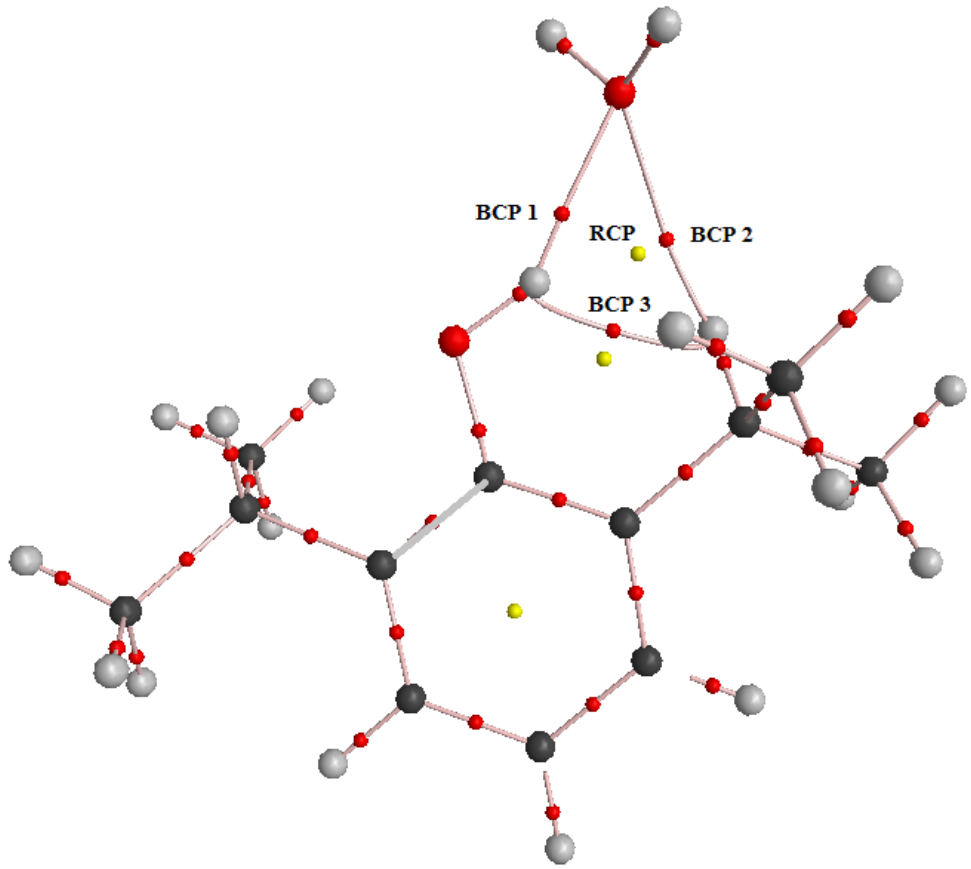

Fig. 5.5: The AIM analysis for the $G^{\pm}G^{\mp}$ Ppf-W complex

Table 5.5: AIM analysis of the bond critical points

BCP	$\rho(r_c)$	$\nabla^2\rho(r_c)$	λ_1	λ_2	λ_3	$\lvert[\lambda_1/\lambda_3]\rvert$	$\lvert[\lambda_1/\lambda_2]-1\rvert$
BCP1	0.0227	0.0878	-0.03025	-0.02845	0.14647	0.206	0.0633
BCP2	0.0010	0.0328	-0.00906	-0.00549	0.047403	0.191	0.649
BCP3	0.0160	0.0604	-0.01627	-0.00896	0.085576	0.190	0.817

Thus the interaction between the two units is shows a combination of inter and an intra molecular hydrogen bonding for this complex. A similar trend is also seen for the W-Ppf and the H-π complex for this conformer.

5.7 Natural Bond Orbital (NBO) Analysis

NBO analysis was performed on the G09 suite of programs to understand the orbital interactions involved in the H-bonded complexes of H_2O and propofol. The activity of the lone pair of electrons in H_2O as a proton donor and propofol as a proton donor plays a crucial role in these interactions. The second order perturbation energy, reported in this section ($E^{(2)}$), $[E_{(j)}-E_{(i)}]$ is the energy difference between the donor and acceptor orbitals involved in the interaction and $[F_{(i,j)}]$ the overlap between the two orbitals. The perturbation energy is directly proportional to orbital occupancy and the square of the overlap integral between the donor and acceptor orbitals, inversely proportional to the difference in energy of the donor and acceptor orbitals. The magnitude second order perturbation energies of the system help in identifying the interactions under consideration. **Table 5.5** gives the bonding patterns in the complexes.

Table 5.5: NBO analysis and the second order perturbation energies at MP2/6-311++g(d,p)

	Ppf-W	**W-Ppf**	**H-π**
EE'			
Involved interaction	(LP) O32- (BD*) C27-H30	(LP) O10-(BD*) O32-H34	Interaction of the **π e⁻** cloud with H33 & H34
$E^{(2)}$	11.2	4.8	
$G^{\pm}E'$			
Involved interaction	(LP) O32- (BD*) C27-H30	(LP) O10-(BD*) O32-H34	Interaction of the **π e⁻** cloud with H33 & H34
$E^{(2)}$	10.8	5.7	
$EG^{\pm}$			
Involved interaction	(BD)O32-H34-(BD*) C27-H30	(LP) O10-(BD*) O32-H34	Interaction of the **π e⁻** cloud with H33 & H34
$E^{(2)}$	22.0	4.3	
$G^{\pm}G^{\mp}$			
Involved interaction	(LP) O32- (BD*) O10-H11	(LP) O10-(BD*) O32-H34	Interaction of the **π e⁻** cloud with H33 & H34 and (LP) O32- (BD*) O10-H11
$E^{(2)}$	7.63	4.2	4.3
$G^{\pm}G^{\pm}$			
Involved interaction	Optimizes to **$G^{\pm}G^{\mp}$** Ppf-W	(LP) O10-(BD*) O32-H34	Interaction of the **π e⁻** cloud with H33 & H34
$E^{(2)}$		4.4	

The NBO analysis of the $G^{\pm}G^{\mp}$ Ppf-W complex, which has been identified experimentally in the matrix, clearly indicates the delocalization of electron density of the lone pair orbital O32 atom of H_2O molecule into the antibonding orbital of the phenolic O10-H11 bond. This clearly indicates that propofol acts like a Lewis acid, accepting electrons from the lone pair of the O atom located on the H_2O molecule. The trend remains the same in other Ppf-W complexes.

In case of the H-π complexes, there is an interaction between the of π cloud of the propofol system with the H of H_2O. The molecular orbitals of the propofol corresponding to the aromatic π cloud participate in the interaction by providing electron density to the hydrogen atoms of the H_2O. In most conformers, in case of the H- π complex, this is the only involved interaction.

However, an interesting complex is the $G^{\pm}G^{\mp}$ **{**H-π + Ppf-W**}** complex. The structure of this complex shows a dual interaction with the phenolic –OH group pushed out of the aromatic plane, where H11 interacts with O32 forming a Ppf-W like complex and the H32 and H33 coming in to interact with the π e^- density of the propofol aromatic ring. This complex, as seen from the second order perturbation energy values, has a weak interaction of the H_2O O32 lone pair with the antibonding orbital of the O10-H11 bond.

5.8 Energy Decomposition Analysis

Energy decomposition analysis helps us to understand the physical origin of various components of the interaction energies in a complex. It decomposes the interaction energy into electrostatic, exchange-repulsion, polarization and dispersion components. The LMOEDA scheme of analysis was employed using GAMESS suite of the programs. **Table 5.6** shows the components of the interaction energies

Since the major component of the stabilizing interaction is electrostatic in nature, one can comment on the strongly hydrogen bonded interaction that is present in such systems. It is clear that for the $G^{\pm}G^{\mp}$ system

Table 5.6.: LMOEDA analysis of the complexes obtained at the MP2/6-311g++(d,p) level of theory. All energy values are in kcal/mol.

Complex	**Electrostatic energy**	**Exchange energy**	**Repulsion energy**	**Polarization energy**	**MP2 Dispersion**	**Total interaction**
PPf-W(EE')	-8.29	-10.29	17.81	-2.00	-1.66	-4.43
W-PPf(EE')	-8.35	-11.49	20.29	-2.55	-1.83	-3.94
H-π PPf(EE')	-5.38	-8.76	14.54	-1.43	-2.95	-3.98
PPf-W($G^{\pm}E'$)	-5.53	-8.94	14.96	-1.64	-2.81	-3.96
W-PPf($G^{\pm}E'$)	-8.07	-10.58	19.00	-2.66	-1.56	-3.87
H-π PPf($G^{\pm}E'$)	-8.35	-11.49	20.29	-2.55	-1.83	-3.94
PPf-W($EG^{\pm}$)	-9.46	-11.16	19.61	-2.61	-1.55	-5.16
W-PPf($EG^{\pm}$)	-8.10	-11.35	19.90	-2.45	-1.92	-3.93
H-π PPf($EG^{\pm}$)	-8.35	-11.49	20.29	-2.55	-1.83	-3.94
PPf-W($G^{\pm}G^{\mp}$)	-9.57	-11.33	19.94	-2.67	-1.55	-5.16
W-PPf($G^{\pm}G^{\mp}$)	*	*	*	*	*	*
{Ppf-W+ H-π PPf} ($G^{\pm}G^{\mp}$)	-10.55	-12.85	22.37	-2.60	-2.48	-6.12
PPf-W ($G^{\pm}G^{\pm}$)	**Optimizes to *$G^{\pm}G^{\mp}$-Ppf-W***					
W-PPf($G^{\pm}G^{\pm}$)	-7.17	-8.86	15.57	-2.03	-1.35	-3.83
H-π($G^{\pm}G^{\pm}$)	-4.74	-8.15	13.53	-1.43	-2.98	-3.77

* *Convergence criteria not met.*

5.9 Discussion

Based on our experiments and our computations, we have been able to identify the global minimum for the 1:1 propofol-H_2O system in the matrix. The vibrational assignment of the spectra clearly indicates that the $G^{\pm}G^{\mp}$ Ppf-W complex is identified in the matrix. These results agree well with the findings of Lessari et. al and Fernandez et. al.[8,11,13-15] Unlike the Benzene-H_2O system,[61] the movement of the H_2O molecule on the ring π-e^- cloud is restricted by the presence of the phenolic –OH and the iPr groups.

The propofol-water system behaves similar to the phenol-H_2O system. Studies on phenol-H_2O by Gor et. al using matrix isolation and *ab initio* studies identified three complexes computationally; phenol as a proton donor, H_2O as a proton donor and a H-π

complex. Experimentally the complex identified in the matrix was the one where phenol served as a proton donor. The phenolic –OH being more acidic than water is consistent with the finding that the complex obtained with phenol as a proton donor is the global minimum for the system under consideration.

Propofol, a phenol derivative is expected to show similar chemistry but with subtle differences because of the effect of the i-Pr groups ortho to the –OH group. The effects of the i-Pr group include through space interaction of the methyl groups of the i-Pr moiety with the phenolic –OH and consequent alteration of the acidity of the phenolic –OH. The molecule also exhibits a variety of conformations that accounts for a rich landscape for the ground state PES for the 1:1 complex system. In our experiments, we have identified the global minimum which is the $G^{\pm}G^{\mp}$ Ppf-W complex.

LMOEDA, NBO and AIM analysis support the fact that a strong hydrogen bond is formed between propofol and the H_2O molecule and accounts for the interaction of the two species. The overall chemistry of the molecule with respect to phenol is not very different but the existence of conformers and other binding sites for the H_2O molecule makes the problem interesting and challenging.

An important insight from this study that we obtain may ultimately be linked to the biological activity of the system. The global minimum structure obtained from matrix isolation studies indicate a stable orientation of the molecule in the $G^{\pm}G^{\mp}$ Ppf-W form. This form may be linked to the activity of the molecule in cases where hydrogen bonding plays a critical role. Since, propofol is known to dock onto the tyrosine and threonine residues of the $GABA_A$ receptor, it is quite possible that conformational orientation of the molecule may play a very critical role for the selective binding of the molecule onto its biological residues. This study provides the first step to understand and develop ideas that might be involved during hydrogen bonding which may lead to the anaesthetic action of this medically significant system.

Chapter 6

Summary and conclusions

6.1 Summary

Matrix isolation infrared spectroscopy, which has been shown to be a powerful tool to study weak interactions and conformers, was used in the conformational analysis of propofol and the study of propofol's 1:1 hydrogen bonded complexes with H_2O. In order to corroborate experimental data, computations were also performed. Geometry optimization algorithms, harmonic analysis and frequency calculations are critical to the understanding of experimental data and such calculations were performed on the Gaussian09 suite of programs. Calculations employing various levels of theory such as the B3LYP, M06-2X and MP2 together with 6-311++g(d,p) and the aug-cc-pVDZ basis sets were performed. AIM analysis, LMOEDA and NBO analysis were also performed to understand the nature of interactions that were under consideration.

Conformational analysis yielded five stable conformers computationally, while three were identified in experiments. These include the $G^{\pm}G^{\mp}$, $G^{\pm}G^{\pm}$, $EG^{\pm}$, $G^{\pm}E'$ and EE'conformers. They are named according to the relative orientation of the methyl and hydrogen atoms of the isopropyl groups on propofol with respect to the aromatic ring. Earlier reports available in the literature do not clearly resolve these conformers and our work is, to the best of our knowledge, the first report of conformer resolution in propofol. . Our *ab intio* computations and experiments corroborate the presence of the $G^{\pm}G^{\mp}$, $G^{\pm}G^{\pm}$ and the $EG^{\pm}$ conformers in the matrix. The $G^{\pm}E'$ and EE' conformers could not be observed in the experimental spectrum due to their low populations.

Fourteen 1:1 hydrogen bonded complexes of propofol with H_2O were obtained computationally, of which the global minimum structure was identified in the matrix. Evidence for the hydrogen bonded complex was obtained from the shifts in the stretching frequency of the O-H group of phenol in propofol. The experimental results were corroborated by computations. . LMOEDA, NBO and AIM analysis helped us to classify the strength and nature of involved interactions in play.

Propofol interaction with water presented a rich and diverse landscape of hydrogen bonded isomers, and the work is clearly important as it sheds light on the non-covalent interactions that leads to its biological activity and its anesthetic action.

6.2 Future scope

In order to see if the conformational population could be altered by varying the temperature of the sample prior to deposition, we tried using supersonic expansion coupled with MI-FTIR. This combination of supersonic jet-matrix isolation was demonstrated to be a powerful method by Viswanathan et al[62] to alter conformational population which leads to unambiguous assignments of the conformers in the matrix. Supersonic jet expansion experiments were carried out using Parker Iota One Pulse Driver controlled pulsed valve unit with a backing pressures of 1 bar of matrix gas. However the very low vapour pressure of propofol prevented enough sample to be deposited onto the matrix and hence vibrational features of propofol could not be obtained. Alternate design and instrumental modification may have to be devised to perform supersonic jet-matrix isolation experiments with propofo.

In the case of 1:1 hydrogen bonded complexes with H_2O, there remains an avenue for assignment of features in and around the –CH stretch regions. The spectra needs to be analysed more carefully supported by more experiments to assign other vibrational features if seen. Though isotopic analysis has been a part of the experiments reported in this work, experiments to assign the –OD shift in the D_2O spectrum need to be analysed and assigned. Overall, the system is open for exploring frontiers and horizons that can strengthen and the obtained and discussed results in this work.

The system can also be explored for higher clusters and formation of 1:n (n=2,3..) complexes of propofol and H_2O. Since amino acid residues also exhibit hydrogen bonding patterns via N atoms, it is worthwhile to explore the interaction of propofol with nitrogen analogues like NH_3 as a part of future endeavors.

Bibliography

[1]Drug Info for Propofol : http://www.drugbank.ca/drugs/DB00818

[2]Tripani G., Altomore C., Sanna E., Biggio G., Liso G.; Current Medicinal Chemistry, 2000, 7, 249-271

[3]Morgan DJ, Campbell GA, Crankshaw DP; British Journal of Clinical Pharm., 1990, Jul:(30) (1), 144-148

[4]Kim Christopher J. , *American Criminal Law Review,* **2014**, 51, 517-40

[5] Medicines.org - "Diprivan-1%" : https://www.medicines.org.uk/emc/medicine/2275

[6] "Propofol Composition" United States Patent Number: 6,140,374; Date of Patent: Oct. 31, **2000**

[7]ICI 35868 (Diprivan): The new intravenous anaesthetic; Kay B., Stephenson D. K.; *Anaesthesia*, **1980**, Vol 35, 1182-87

[8]Lesarri A.; Shipman S. T.; Neil J., Brown G.G.; Suenram R. D.; Kang Lu, Caminati W.; Pate B. H.; *J. Am. Chem. Soc.*, **2010**, 132 (38), pp 13417– 13424

[9]Gor G. Y.; Tapio S.; Domanskaya A. V;, Räsänen M.; Nemukhin A.V.; Khriachtchev L.; *Chemical Phys. Lett*., **2011,**(517), 1–3, 9–15

[10]Sundarajan K.; Ramanathan N. ; *Journal of Mol Str*, **2009** Vol 920, (1–3), 369–376

[11]León I.; Lesarri A.; Millán M.; Castaño F.; Cocinero E. J.; Fernández J. *Phys. Chem. Chem. Phys*., **2012,** 14, 8956-63

[12]Yip G. M. S., Zi-Wei Chen, Edge C. J., Smith E. J; Dickinson R., Hohenester E., Townsend R., Fuchs K., Sieghart W., Evers A., Franks N.P ; *Nature Chemical Biology*, **2013**, 9, 715–720

[13]León I.; Lesarri A.; Millán M.; Castaño F.; Cocinero E. J.; Fernández J. *Journal of Phys. Chem. A*, **2012,** 116, 8934-41

[14]León I.; Lesarri A.; Millán M.; Castaño F.; Cocinero E. J.; Jaeqx S.;Rijs A. M.; Fernández J. A.; *Phys. Chem. Chem. Phys*., **2012,** 14, 4398-4409

[15]León I.; Lesarri A.; Millán M.; Castaño F.; Cocinero E. J.;Usabiaga I.; Fernández J. A.; *Phys. Chem. Chem. Phys*., **2014,** 16, 16968-16975

[16]Jeffery G. A.; *Hydrogen bonding in Biological Structures*; **1991**, Springer; Berlin

[17]Elangannan Arunan1, Gautam R. Desiraju, Roger A. Klein, Joanna Sadlej, Steve Scheiner, Ibon Alkorta, David C. Clary, Robert H. Crabtree, Joseph J. Dannenberg, Pavel Hobza, Henrik G. Kjaergaard, Anthony C. Legon, Benedetta Mennucci, and David J. Nesbitt;. *Pure Appl. Chem.*, **2011**, 83, No. 8, 1637–1641

[18]Jeffery G. A." *An Introduction to Hydrogen Bonding*" **1997,** *Oxford University Press-New York*

[19]Reed A. E.; L. A. Curtiss; F. Weinhold; *Chem. Rev. ,* **1988**, 88, 899-926

[20]Hobza P.; Havlas Z. ; *Chem. Rev,* **2000**, 100, 4253

[21]Epstien L. M.; Shubina E. S.; *Coord. Chem. Rev.*, **2002**, 231, 165-81

[22]Epstien L. M.; Shubina E. S.; Belkova N. V.; Gustul E.I.; *Polish J. of Chem. ,* **2003**, 77, 1371-83

[23]Custelcean R. ; Jackson J. ; *Chem. Rev*., **2001**, 101, 1963-80

[24]Gaussian 09, Revision E.01, M. J. Frisch, G. W. Trucks, H. B. Schlegel, G. E. Scuseria et. al.: Gaussian, Inc., Wallingford CT, 2009.

[25]H. E Hallam; *Vibrational Spectroscopy of Trapped Species*, *John Wiley and Sons*, London. **(1973)**.

[26]G.C Pimentel, S. W Charles; Pure and Appl. Chem **1963**, 7, 11

[27]A. J. Barnes and H. E. Hallam; *Q. Rev. Chem. Soc*., **1969**,23, 392-409

[28]A J Hinchcliffe, S28tephen Cradock; *Matrix Isolation: A Technique for the Study of Reactive Inorganic Species, Cambridge University Press* (**1975**)

[29]W. Press, B. Janik, H. Grimm, Z. ; *Phys-B Condensed Matter* **1982**, 49, 9-16

[30]Lisa George, K. Sankaran, K. S. Viswanathan, and C. K. Mathews; ***Applied Spectroscopy*** **1994**, Vol. 48, Issue 1, 7-12

[31]Gary L. Johnson and Lester Andrews; *J. Am. Chem. Soc*., **1980**, 102, 18, 5736-41

[32]Viswanathan, K., Sankaran, K. and Sundararajan, K.; *Matrix Isolation Spectroscopy in Atmospheric Chemistry, Encyclopaedia of Analytical Chemistry*, (**2006**).

[33]A. J Barnes; *J. Mol Str,* **1980**, Volume 60, Pages 343-346

[34]A. D Buckingham; *Proc. Roy. Soc. (London) A,* **1958**, 248, 169

[35]J. A. Warren, G. R. Smith, W. A. Guillory; *J. Chem. Phys.*, **1980**, 72, 4901.

[36]B. R. Carr, B. M. Chadwick, C. S. Edwards, D. A. Long, G. C. Wharton, *J. Mol.Str*., **1980** , 62, 291.

[37]Stuart, B.; *Infrared Spectroscopy. Kirk-Othmer Encyclopedia of Chemical Technology.*

*(***2005**)

[38]Bruker Tensor 27 FTIR Instruction Manual

[39]HC-4E1 Helium Compressor; Technical Manual, Sumitomo (SHI) Cryogenics of America, Inc.

[40]http://arscryo.com/LT3B.html : Cryostat Classifications

[41]A. Szabo, N.S. Ostlund*; Modern Quantum Chemistry: Introduction to Advanced Electronic Structure Theory; Courier Corporation Inc*

[42]P. Hohenberg, W. Kohn; *Phys. Rev*., **1964**, 136, B864

[43]W. Kohn, L. J Sham; *Phys. Rev*., **1965**, 140, A1133

[44]J. P Foster, F. Weinhold; *J. Am. Chem. Soc.,* **1980**, 102, 7211-18

[45]M. W Schmidt, K. K Baldridge, J. A Boatz, S. T. Elbert, M. S. Gordon, J. H. Jensen, S. Koseki, N. Matsunaga, K. A Nguyen, S. Su, T. L Windus, M. Dupuis, J. A Montgomery, *J. Comp. Chem*, **1993**, 14, 1347-63

[46]L. Turi, J. J. Dannenberg, *J. Phys. Chem.*, **1995**, 99, 639

[47] Shavitt, I., The History and Evolution of Gaussian Basis Sets. *Isr. J. Chem*., **1993**, 33: 357–367.

[48]Thorn H. Dunning, Jr, *J. Chem. Phys.*, **1988**, Vol. 90, No.2, 1008

[49]Robert G. Parr, Yang Weitao; *Density-Functional Theory of Atoms and Molecules; Oxford University Press London*

[50]Scuseria GE, Staroverov VN, **2005**; Dykstra CE, Frenking G, Kim KS, Scuseria GE (eds) *Theory and application of computational chemistry*: the first 40 years. Elsevier, Amsterdam, 669–724

[51]Yan Zhao, Donald G. Truhlar; *Theor Chem Acc.,* **2008**, 120:215–241

[52]Pavel Hobza, ZdenvÏk Havlas, *Theor Chem Acc.*, **1998**, 99:372-77

[53]Pavel Hobza, ZdenvÏk Havlas, *Theor Chem Acc.*, **1998**, 99:372-77

[54]Richard W. Bader, *Atoms in Molecules: A Quantum Theory (International Series of Monographs on Chemistry)*

[55]Eric D. Glendening; *J. Phys. Chem. A,* **2005,** *109,* 11936-11940

[56]Iker Leon , Emilio J. Cocinero, Judith Millán, Sander Jaeqx, Anouk M. Rijs, Alberto Lesarri, Fernando Castaño and José A. Fernández; *Phys. Chem. Chem. Phys*, **2012**, **14**, 4398-4409

[57]L. George, K. S. Viswanathan, S. Singh; *J. Phys. Chem. A*, **1997**, *101* (13), pp 2459–2464

[58]Singh P.C., Bandyopadhyay B., Patwari G.N.; *J. Phys.Chem. A.*, (**2008**), 112, 3360-3363

[59]Karir G., Viswanathan K.S.; *J. of Mol. Str.*, (**2016**), 1107, 145-156

[60]Koch, U.; Popelier, P. L. A.. *J. Phys. Chem.*(**1995**), 99, 9747−9754.

[61]Li S., Cooper V.R. , Thonhauser T., Puzder A., Langreth D.C.; *J. Phys. Chem. A,* (**2008**), 112, (38), 9031-6

[62]L. George, K. S. Viswanathan, S. Singh; *J. Phys. Chem. A*, **1997**, *101* (13), pp 2459–2464